AD A116671

AFWAL-TR-82-2044

LOCAL LEADING EDGE DAMAGE FROM HARD PARTICLE AND SOFT
BODY IMPACTS (TASK IV B)

Robert S. Bertke

University of Dayton Research Institute
Dayton, Ohio 45215

May 1982

Interim Report for Period 1 January 1979 - 1 December 1980

DTIC FILE COPY

JUL 7 1982

A

AERO PROPULSION LABORATORY
AIR FORCE AERONAUTICAL LABORATORIES
AIR FORCE SYSTEMS COMMAND
WRIGHT-PATTERSON AIR FORCE BASE, OHIO 45433

82 07 07 004

SANDRA K. DRAKE
Project Engineer

ISAK J. GERSHON
Technical Area Manager,
Propulsion Mechanical Design

FOR THE COMMANDER

J. SHIPMAN, MAJ. USAF
Deputy Director, Turbine Engine Division

REPORT DOCUMENTATION PAGE		READ INSTRUCTIONS BEFORE COMPLETING FORM
1. REPORT NUMBER AFWAL-TR-82-2044	2. GOVT ACCESSION NO. AD-A116671	3. RECIPIENT'S CATALOG NUMBER
4. TITLE (and Subtitle) LOCAL LEADING EDGE DAMAGE FROM HARD PARTICLE AND SOFT BODY IMPACTS (TASK IVB)		5. TYPE OF REPORT & PERIOD COVERED Tech. Report Oct. 1977 - June 1980
		6. PERFORMING ORG. REPORT NUMBER UDR-TR-81-20
7. AUTHOR(s) R. S. Bertke		8. CONTRACT OR GRANT NUMBER(s) 200-4BA-14K-47844 (GE) F33615-77-C-5221
9. PERFORMING ORGANIZATION NAME AND ADDRESS University of Dayton Research Institute 300 College Park Ave. Dayton, Ohio 45469		10. PROGRAM ELEMENT, PROJECT, TASK AREA & WORK UNIT NUMBERS 62203F, 3066, 12, 33
11. CONTROLLING OFFICE NAME AND ADDRESS General Electric Company Evendale Plant - Aircraft Engine Group Evendale, OH 45215		12. REPORT DATE May 1982
		13. NUMBER OF PAGES 94
14. MONITORING AGENCY NAME & ADDRESS(if different from Controlling Office) Aero-Propulsion Laboratory Wright-Patterson Air Force Base Dayton, Ohio 45433		15. SECURITY CLASS. (of this report) Unclassified
		15a. DECLASSIFICATION/DOWNGRADING SCHEDULE

16. DISTRIBUTION STATEMENT (of this Report)

Approved for public release; distribution unlimited

17. DISTRIBUTION STATEMENT (of the abstract entered in Block 20, if different from Report)

18. SUPPLEMENTARY NOTES

19. KEY WORDS (Continue on reverse side if necessary and identify by block number)

Foreign object damage, leading edge impact damage, local damage, hard particle impacts, soft-body impacts, bird impacts, titanium, stainless steel, boron/aluminum composite.

20. ABSTRACT (Continue on reverse side if necessary and identify by block number)

This report describes a study to experimentally determine the leading edge local response of typical blade materials to impact loading and derive analytical/empirical models of the response. The three fan blade type materials investigated were the J79 blade material of 403 stainless steel, the F101 blade material of 8Al-1Mo-1V (8-1-1) titanium and the APSI metal matrix blade material of boron/aluminum. The local leading edge

DD ₁ FORM ₇₃ 1473   EDITION OF 1 NOV 65 IS OBSOLETE

damage problem was investigated on the three materials using glass beads, steel spheres, granite pebbles, ice, and artificial birds as the impactors. The resulting specimen damage for each impactor type and size was characterized by identifying the damage mode and quantifying the damage by making various damage measurements.

The concept of geometric scaling was investigated by performing a series of impact tests using different leading edge thick nesses and projectile sizes. The damage for the two thick- nesses was very similar in appearance; however, the concept of geometry scaling did not seem to work as well as expected.

The effects of preload (centrifugal loading in a blade) was also investigated. Tensile stresses of 12 and 15 Ksi were used in these impact tests and the results showed that damage is likely to be less due to centrifugal loading than for static unloaded impact tests.

This report describes a contractual work effort conducted for the General Electric Company, Aircraft Engine Group under Purchase Order No. 200-4BA-14K-47844 which is a subcontract of F33615-77-C-5221.

This report covers work conducted during the period of October 1977 to June 1980 and is part of Task IV B.

The GE Program Manager was Mr. Joe McKenzie and the Principal Investigator was Mr. Al Storace. The work reported herein was performed under the direction of Mr. Robert S. Bertke, Impact Physics Group of the Experimental and Applied Mechanics Division, University of Dayton Research Institute.

Technical support was provided by Mr. Charles E. Acton in the study.

TABLE OF CONTENTS

TABLE OF CONTENTS (Continued)

LIST OF ILLUSTRATIONS

LIST OF ILLUSTRATIONS (CONTINUED)

LIST OF ILLUSTRATIONS (CONCLUDED)

LIST OF TABLES

SECTION I

INTRODUCTION

Modern gas turbine engines for aircraft utilize fan blades
made from homogeneous metals. Advanced engine concepts currently
under development envision using fan blades made from intermetallic
and nonmetallic composite materials. An important property of fan
blade materials is the resistance of the material to impacts from
birds, stones, ice balls, and other items. The damage inflicted
by such impacts is known as foreign object damage (FOD).

Impacts on fan blades can be classified either as hard-body
or soft-body impacts. The phenomena associated with hard objects
(such as munitions) and soft objects (such as birds) are fundamen-
tally different. Hard objects tend to retain their size and shape
during the impact process. This results in intense localized dam-
age at the impact site with relatively slight effects at larger
distances. Soft projectiles deform grossly upon impact and pro-
duce less localized damage but significantly greater effects at
large distances from the impact site. The damage at greater dis-
tances from the impact site is largely due to the total impulse
transferred to the blade during the impact.

The FOD problem of fan blade materials can be divided into
two separate problem areas. One concerns the local blade damage
and the second deals with the structural damage. Local damage
occurs during the impact and is confined to within one or two pro-
jectile diameters of center of the impact site. Structural damage
occurs at later times and at points which are, in general, well
away from the impact site.

The purpose of Task IV, Material Response and Failure
Criteria, was to experimentally determine the response of various
materials to impact loading in terms of strain rates and to derive
analytical/empirical models of the response for use with the Task II
analytical models of the program. Both gross structural damage and
leading edge damage were investigated. Also material screening
tests for impact response were established.

1

Three subtasks were involved in the Task IV effort. The first subtask (IVA) was concerned with gross structural damage. The approach in this subtask was to develop a material response model which accurately describes the failure phenomena which take place in FOD events. The second subtask (IV B) was concerned with the generation of empirical design data for leading edge impacts onto three typical blade designs. The final subtask (IV C) was concerned with the development of screening tests so that candidate fan blade materials which may possess superior FOD resistance could be quickly identified.

This report describes an experimental study concerned with the second subtask effort (IV B) which deals with local leading edge damage. In this subtask, tests were conducted to determine and quantify the damage caused by leading edge impacts for a range of pertinent impact conditions.

SECTION II
EXPERIMENTAL PROGRAM

The experimental program involved conducting non-rotating impact tests on small test specimens of blade materials. Three types of blade materials, geometries, and sizes were to be investigated using ice, glass beads, granite pebbles, and substitute bird materials as the impactors. The impactors were gun launched to impact the leading edge of the test specimens.

2.1 STUDY OBJECTIVES AND APPROACH

The overall objectives of this study were to experimentally determine the leading edge local response of the various materials to impact loading and derive analytical/empirical models of the response for use with the analytical models of the program. The three blade types investigated were the J79 blade using 403 stainless steel; the F101 blade using 8 Al-1Mo-IV (8-1-1) titanium; and the APSI metal matrix boron/aluminum blade. Since only the local damage aspect was to be investigated in this subtask, the test specimen size was determined by the projectile size. The geometries of the leading edges of the specimens were similar to the geometries of the three blade types at the 50 percent span. For example, the material, leading edge thickness, taper angle, specimen thickness, and width of the test specimens were identical to the actual blades at the 50 percent span level.

The test parameters which were to be investigated are listed in Table 1. Slice equivalents of 57-85 g (2 to 3 ounces) and 680 g (1.5 pound) birds were to be employed using the projectile material of microballoon gelatin with 10 to 15 percent porosity. Previous work has demonstrated that this material very effectively reproduces the loads delivered by actual birds. (References 1, 2, 3, and 4). The ice spheres to be utilized was 2.54 cm (1.0 - inch) diameter which may be considered as representative of hail ingestion. The long ice cylinders to be used was 2.54 cm (1.0 inch) diameter by 10.16 cm (4.0 inch) long slices to simulate the effects of the

3

TABLE 1

LEADING EDGE IMPACT TESTS PARAMETERS

Impactors	Artificial Birds	57-85 gram (2 to 3 ounce) slices 680 gram (1.5 pound)
	Ice	2.54 cm (1 inch) diameter spheres 2.54 cm (1 inch) diameter x 10.16 cm (4 inch) long slice
	Hard Particles	0.64 cm (0.25 inch) diameter "standard" pebble 1.52 mm (60 mil) glass beads 0.76 mm (30 mil) glass beads
Targets	J-79 403 Stainless Steel 50% Span Geometry	Nominal thickness One-half thickness
	F-101 8-1-1 Titanium 50% Span Geometry	Nominal thickness One-half thickness
	Advanced Composite APSI Boron-Aluminum 50% Span Geometry	Nominal thickness One-half thickness
Velocities	Typical of 70% Span Typical of 30% Span	

impact of a slice from an ice slab. The hard particles to be utilized were 0.64 cm (0.25 inch) diameter granite pebble and glass beads of 0.76 and 1.52 mm (30 and 60 mil.) diameters. The granite pebble had a standard cone-cylinder-cone configuration (shown in Figure 1) which has been developed to evaluate the vulnerability of ballistic missile components to pebble impact. This range of impactors is representative of the types of objects commonly ingested into engines. The designers must be able to adequately design against these threats.

As the tests were conducted, some changes in the test parameters were required to obtain meaningful data. For example, the glass beads were breaking up for high velocity impacts and steel spheres were substituted. Also, the 680 gram (1.5 pound) bird impacts were eliminated because of the amount of damage received from the 85 gram (3 ounce) impacts. In addition, the size of the steel spheres was increased to 1.52 and 3.17 mm (60 and 125 mil.) diameter sizes resulting from minimal damage received in the 0.76 mm (30 mil.) impacts. These changes in the study are described in detail in a later section of this report.

2.1.1   Specimen Materials and Geometries

As indicated earlier, the three blade types to be investigated were the J79 blade using 403 stainless steel, the F101 blade using 8-1-1 titanium, and the APSI blade using boron/aluminim material. These choices correspond to those which would be investigated analytically and experimentally in other tasks of the overall program. The half-thickness targets shown in Table 1 are to investigate scaling effects and the use of subscale testing to generate local damage data. The leading edge geometries of the test specimens are similar to the geometries of the actual blades at the 50 percent span location. The material, leading edge thickness, and width of the test specimens are identical to the various blade types.

2.1.1.1   J79 Blade Specimens

The test specimens simulating the J79 blade were fabricated of 403 stainless steel material for the nominal

5
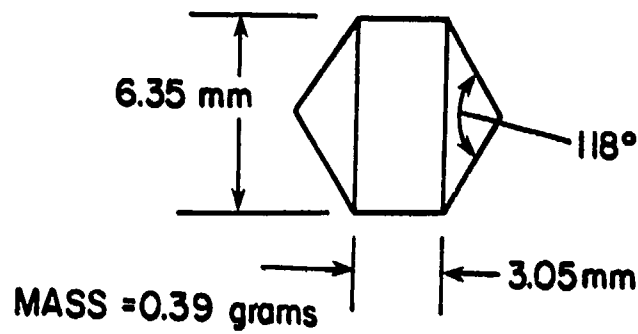
Figure 1.   Sketch of Granite Pebble Utilized in Testing.

thickness specimens and 410 stainless steel for the one-half thickness specimens. Both steels were used in the annealed condition. The 410 stainless steel was substituted because the 403 material was unavailable in the desired thickness required to fabricate the subscale thickness specimens. Figure 2 gives the cross-sectional geometry for the nominal and half-thickness specimens. The length of the specimens depended on the impactor size. The artificial bird impacts were conducted on 45.7 cm (18.0-inch) long specimens while the smaller size projectiles were utilized on 22.9 cm (9-inch) long specimens. The leading edge thickness for the nominal thickness specimens was 1.22 mm (0.048-inches) and the maximum thickness was 4.6 mm (0.181-inches) at the chord center. For the one-half-thickness specimens, the leading edge thickness was 0.61 mm (0.024-inches) and the maximum thickness was 2.3 mm (0.090-inches).

2.1.1.2 F101 Blade Specimens

The test specimens simulating the F101 blade were fabricated from 8-1-1 titanium material. Figure 3 gives the cross-sectional geometry for the nominal and one-half thickness specimens. Again, the length of the specimens depended upon the impactor size. The leading edge thickness for the nominal thickness specimens was 0.81 mm (0.032-inches) and the maximum thickness was 4.3 mm (0.168-inches). The one-half thickness specimens had a leading edge thickness of 0.41 mm (0.016-inches) and a maximum thickness of 2.13 cm (0.084-inches). All of the titanium specimens were in the shot peened condition to an intensity of 0.005-0.008 N using glass beads 0.58-0.84 mm (0.023-0.033-inch) diameter.

2.1.1.3 APSI Blade Specimens

Test specimens of boron/aluminum material simulating the APSI blade were fabricated by General Electric Company. Figure 4 shows a sketch of the symmetical test specimens. The leading edge thickness for the nominal thickness specimens was 0.64 mm (0.025-inches) and the maximum thickness was 3.81 mm (0.1__-inches). The leading edge thickness for the one-half thickness specimens was 0.30 mm (0.012-inches) and the maximum thickness was 3.51 mm (0.138-inches). The length of the specimens was 12.7 cm (5.0-inches). The specimens had nickel plating on the leading edge

7

STAINLESS STEEL

NOMINAL THICKNESS SPECIMEN

45.72 cm LONG

HALF-THICKNESS SPECIMEN

22.86 cm LONG
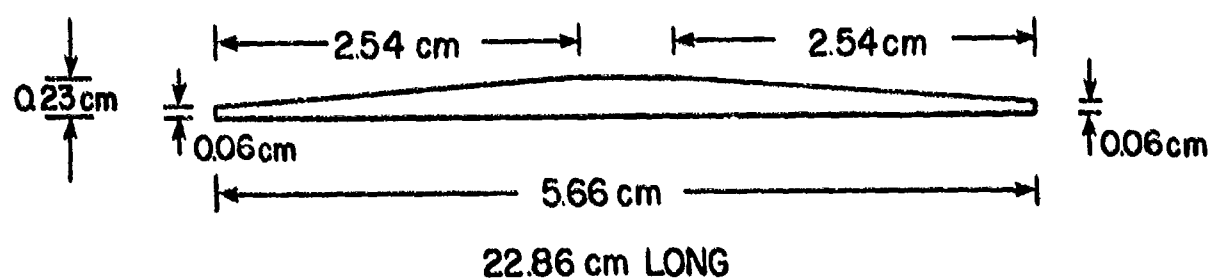
Figure 2.   Sketch of Cross-Sectional Geometry of the Stainless
Steel Test Specimens.

8

TITANIUM
NOMINAL THICKNESS SPECIMEN

Figure 3. Sketch of Cross-Sectional Geometry of the Titanium Test Specimens.

9

COMPOSITE NOMINAL THICKNESS SPECIMEN
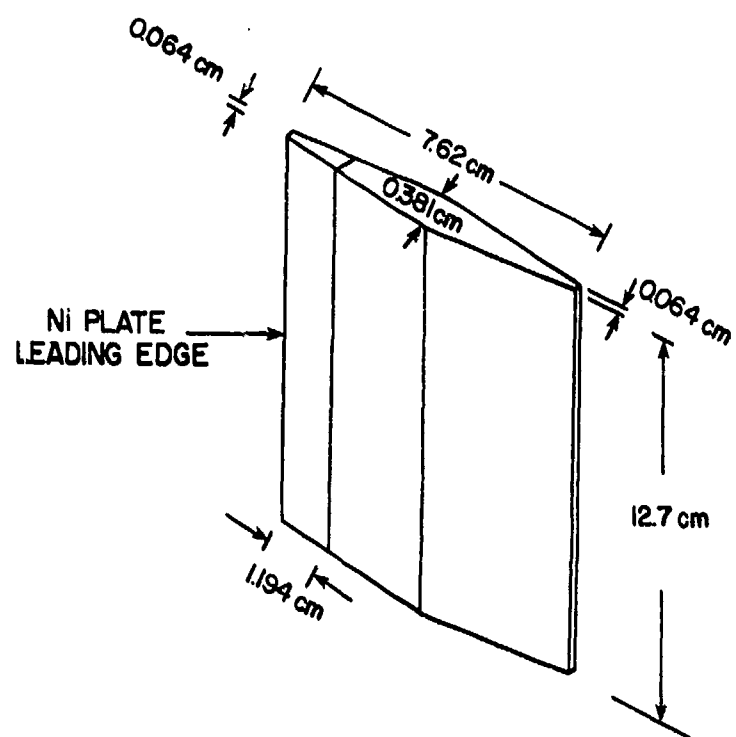
HALF-SCALE SPECIMEN
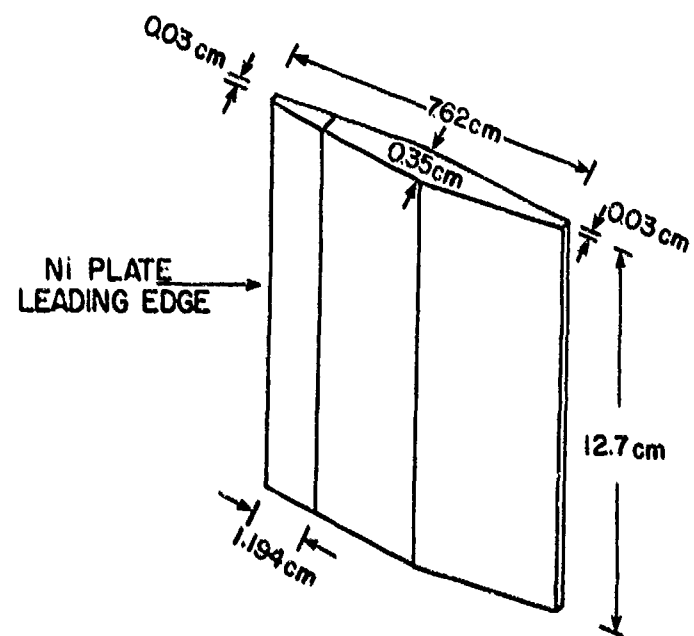
Figure 4.   Sketch of the Symmetrical APSI Test Specimens.

10

and a stainless steel wire mesh outer ply. The symetrical layup used in the specimens was 0°/22°/0°/-22° with the number of plies being sufficient to obtain the desired thickness.

2.1.2   Impact Velocities and Angles

The impact velocities to be used in the study correspond to those which would be typical of an impact at 70 percent span and at 30 percent span at full power settings of the engine during takeoff on each of the blade types. Impacts at the 70 percent span level are representative of the highest velocity impacts experienced by a blade. Impacts at the 30 percent span level are typical of those in the highest stress regions of the blade where it is most vulnerable to the effects of impact degradation.

The impact angles on the various test specimens were to correspond to the impact angles that would occur on the actual blades for a given span location. These impact angles, impact velocities, and bird mass values were determined from the blade geometry, the blade velocity for a given span location, and the aircraft speed. The following paragraphs describe an effort to calculate the projectile-blade relationships for an impact.

2.1.2.1   Test Conditions for Various Blade Types

The effort consisted of deriving bird slice relationships for the bird-blade interface geometry shown in Figure 5. The calculations are for obtaining the maximum bird slice that a row of blades would experience from a large bird impact. The calculations were performed for a starling impact (85 grams) and a large bird impact (680 grams) on the J79, F101, and APSI blades.

Three assumptions are made in the calculations. The first assumption is that the bird geometry is cylinder in shape with a length to diameter ratio equal to two. The second assumption is that the bird density is equal to 0.91 g/cm^3 (0.033 lb/in^3). (See References 1, 2, 3, and 4) The last assumption is that the bird axial velocity is equal to the aircraft velocity. This velocity was assumed to be approximately 61 m/s (200 ft/s) for takeoff and landing situations where FOD strikes are most likely to occur.

11
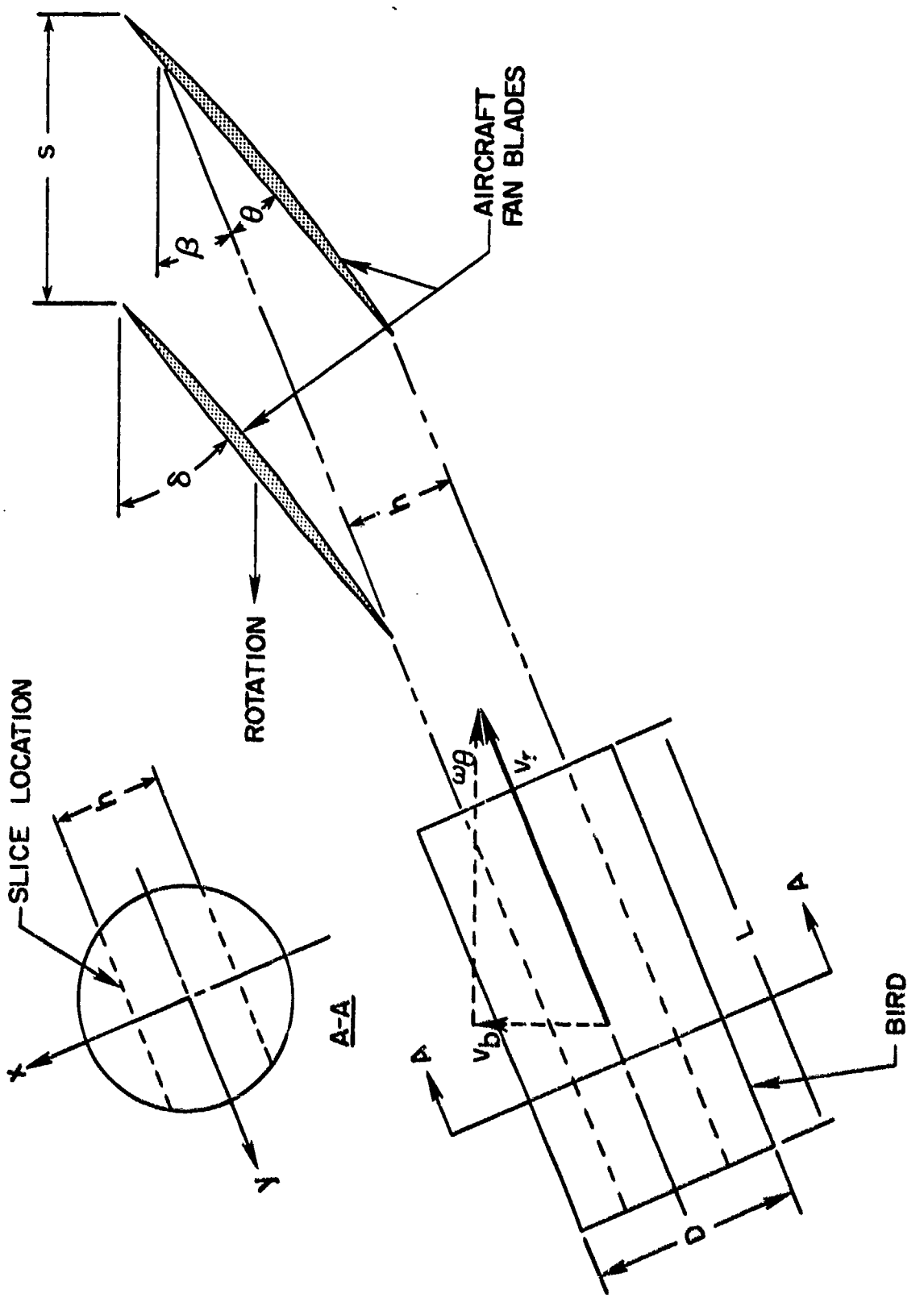
Figure 5. Bird-Blade Interface Geometry.

The input parameters from the blade required
to make the calculations are: (1) the number of blades per stage
(N); (2) the blade rotational speed (n); (3) the span radius where
the impact is to occur (r_i); and (4) the blade orientation angle
(δ).

The bird input parameters necessary are:
(1) the axial velocity of the bird (V_b) which is assumed to be
equal to the aircraft velocity and (2) the bird weight (W_b).

Table 2 gives the general equations
utilized to determine the test conditions (impact velocity, impact
angle, and bird slice weight) for an impact on a particular blade
span location, and bird size.

Tables 3 and 4 give the calculated test
condition parameters for the three blade types. Table 3 gives the
results for a starling (85 g) bird and Table 4 gives the calculations
for a large bird (680 g). Both tables are for impacts at the 30 and
70 percent span locations with the engines at full power settings
during takeoff for each of the blade types.

Three specific investigations were planned
in this effort. The first was to establish a base of damage data.
The second addressed scaling and subscale tests while the third in-
vestigated the effects of preload and possible damage enhancement.
The test conditions proposed in the original test plan are listed
in Table 5. As indicated earlier, as the testing was conducted
and damage results evaluated, some changes in the test conditions
were required to obtain meaningful data. One of the changes in-
volved was the test plan for the boron/aluminum material. The cost
of fabricating specimens limited the number of tests. Table 6 gives
the test conditions in the revised test plan for the metal matrix
composite specimens. In this case, only glass bead impacts would
be conducted in the study.

Another change was substituting chrome steel
spheres for the glass beads because of the glass bead break-up for
impacts at the higher velocities. The reason for this substitution

TABLE 9. GENERAL EQUATIONS UTILIZED TO DETERMINE TEST CONDITIONS

Bird Geometry

Bird Diameter $\qquad D = \sqrt[3]{2W_b/\pi\rho}$ (cm)

Bird Length $\qquad L = 2D$ (cm)

Bird-Blade Interaction Parameters

Relative Velocity $\qquad V_r = (W_\theta^2 + v_b^2)^{1/2}$ (m/s)

Bird Tangential Velocity @ r_i $\qquad W_\theta = 2\pi n r_i/6000$ (m/s)

Bird-Blade Angle Relative to
Tangent @ r_i $\qquad \beta = \sin^{-1} V_b/V_r$ (°)

Blade Tangential Spacing @ r_i $\qquad S = 2\pi r_i/N$ (cm)

Bird Slice Width $\qquad h = S \sin \beta = \dfrac{2\pi r_i}{N} \dfrac{V_B}{V_r}$ (cm)

Bird-Blade Impingement
Angle $\qquad \theta = \delta - \beta$ (°)

Bird Slice Weight $\qquad W_s = \rho L \displaystyle\int_{-\frac{h}{2}}^{\frac{h}{2}} 2\sqrt{\left(\frac{D}{2}\right)^2 - x^2}\, dx$

$$W_s = 2\rho\, D \left[h\sqrt{\left(\frac{D}{2}\right)^2 - \left(\frac{h}{2}\right)^2} + \frac{1}{2}\, D^2\, \sin^{-1}\left(\frac{h}{D}\right) \right]$$

TABLE 3

TEST CONDITIONS FOR STARLING IMPACT

PARAMETER	J79		APSI		F101	
Rotor Speed, n (rpm)	7460		17500		7555	
N$^{\underline{o}}$ Blades, N (-)	21		28		50	
Tip Radius, R_t (cm)	37.21		27.94		56.34	
Root Radius, R_R (cm)	13.23		12.57		29.74	
Span Location (%)	30	70	30	70	30	70
Radius, r_i (cm)	20.42	30.02	17.18	23.33	37.72	48.36
Orientation Angle, δ (°)	72.0	51.0	49.8	27.0	52.5	33.5
Chord Length, C (cm)	5.66	5.66	7.37	7.77	8.38	9.40
Calculated Values						
Blade Tangential Velocity, W_θ (m/s)	159	234	315	428	298	383
Bird Axial Velocity, V_b (m/s)	61	61	61	61	61	61
Relative Velocity, V_r (m/s)	170	242	321	432	304	388
Bird Weight, W_b (g)	85.3	85.3	85.3	85.3	85.3	85.3
Bird Slice Width, h (cm)	2.18	2.26	0.74	0.74	0.94	0.97
Bird Slice Weight, W_s (g)	57.15	58.51	20.41	20.41	25.86	26.31
Bird-Blade Incidence Angle, θ (°)	51.1	36.4	38.8	18.9	41.0	24.0
Angle β (°)	20.9	14.6	11.0	8.1	11.5	9.1
Bird Diameter, D (cm)	3.89	3.89	3.89	3.89	3.89	3.89

TABLE 4

TEST CONDITIONS FOR LARGE BIRD (680g) IMPACT

PARAMETER	J79		APSI		F101	
Rotor Speed, n (rpm)	7460		17500		7555	
N$^{\underline{o}}$ Blades, N (-)	21		28		50	
Tip Radius, R_t (cm)	37.21		27.94		56.34	
Root Radius, R_R (cm)	13.23		12.57		29.74	
Span Location (%)	30	70	30	70	30	70
Radius, r_i (cm)	20.42	30.02	17.18	23.22	37.72	48.36
Orientation Angle, δ (°)	72.0	51.0	49.8	27.0	52.5	33.5
Chord Length, C (cm)	5.66	5.66	7.37	7.77	8.38	9.40
Calculated Values						
Blade Tangential Velocity, W_Θ (m/s)	159	234	315	428	298	383
Bird Axial Velocity, V_b (m/s)	61	61	61	61	61	61
Relative Velocity, V_r (m/s)	170	242	321	432	304	388
Bird Weight, W_b (g)	680.4	680.0	680.4	680.4	680.4	680.4
Bird Slice Width, h (cm)	2.18	2.26	0.74	0.74	0.94	0.97
Bird Slice Weight, W_s (g)	240.41	249.48	81.65	81.65	104.33	104.33
Bird-Blade Incidence Angle, Θ(°)	51.1	36.4	38.8	18.9	41.0	24.4
Angle β (°)	20.9	14.6	11.0	8.1	11.5	9.1
Bird Diameter, D (cm)	7.80	7.80	7.80	7.80	7.80	7.80

TABLE 5

LEADING EDGE IMPACT TEST CONDITIONS (ORIGINAL TEST PLAN)

Damage Data Base Acquisition

	Soft Objects	Hard Objects
Impactors	57-85 g (2-3 ounce) Birds 680 g (1.5 pound) Birds 2.54 cm (1.0 inch) Dia. Ice Spheres 2.54 cm (1.0 inch) Dia. 10.16 cm (4 inch) Long Ice Slab	0.64 cm (0.25 inch) Dia. "standard" Pebble 1.52 mm (60 mil) Glass Bead 0.76 mm (30 mil) Glass Bead

Targets	403 Stainless Steel 8-1-1 Titanium Boron/Aluminum	Nominal Thickness

Velocities	Typical of 70% Span Typical of 30% Span	

Scaling Effects Investigation

Impactors	57-85 g (2-3 ounce) Birds 0.76 mm (30 mil) Glass Beads	

Targets	410 Stainless Steel 8-1-1 Titanium Boron/Aluminum	One-Half Thickness

Velocities	Typical of 70% Span Typical of 30% Span	

Preload Effects Investigation

Impactors	680 g (1.5 pound) Birds	

Targets	403 Stainless Steel 8-1-1 Titanium Boron/Aluminum	Nominal Thickness

Velocities	Typical of 70% Span Typical of 30% Span	

17

TABLE 6

LEADING EDGE TEST CONDITIONS FOR COMPOSITE SPECIMENS (REVISED TEST PLAN

Damage Data Base Acquisition

Impactors	{	0.030" Glass Bead
		0.060" Glass Bead
Target		B/Al (Nominal Thickness
Velocity		Typical of 70% Span

Scale Effects

Impactor	0.030" Glass Bead
Target	B/Al (One-half Thickness)
Velocity	Typical of 70% Span

Preload Effects

No testing. Negligible effect based on previous experience.

18

was to avoid the uncertainty surrounding the effect of projectile break-up upon the damage inflicted on the specimens. In addition, the size of the chrome steel spheres was increased to 1.59 and 3.18 mm (60 and 125 mil) diameter. The reason for this change was of the minimal damage being received for the 0.76 mm (30 mil) impacts.

Also, the 680 g (1.5 pound) bird and ice slab impacts were eliminated from the original test plan. The 85 g (3 ounce) bird impacts were generating a large amount of damage on the specimens and increasing the bird mass in the impacts by a factor of four would result in overpowering the specimens. Since the specimens were flat without camber and twist, the stiffness of the test specimens would be much lower than for the actual blades. The local leading edge damage would also be determined for 680 g (1.5 pound) bird impacts in the Task VI effort of the total program. In regards to the ice slab impacts, several attempts to launch the ice slabs intact on the small bore FOD range were unsuccessful. Due to the acceleration forces in launching the ice slab projectiles, they would break-up upon launch and impact the targets with a spray of small ice particles.

2.2   EXPERIMENTAL SETUP AND PROCEDURES

The impact tests were conducted on one of two FOD impact ranges depending on the projectile size. The smaller range configuration is capable of launching spheres or cylinder up to 3.17 cm (1.25 inch) diameter to velocities of 1219 m/s (4000 ft/s). The second range configuration is capable of launching 2.54 to 7.62 cm (1 to 3 inch) diameter spheres or cylinders up to velocities of 350 m/s (1150 ft/s). A brief description of each range setup is given below.

2.2.1   Small Bore FOD Gun Range

A schematic of the range setup used in the impact testing of the smaller size projectiles is shown in Figure 6. The range setup consisted of a launch tube, velocity measuring system, sabot catch tank, and a target tank. For the smaller projectiles

19
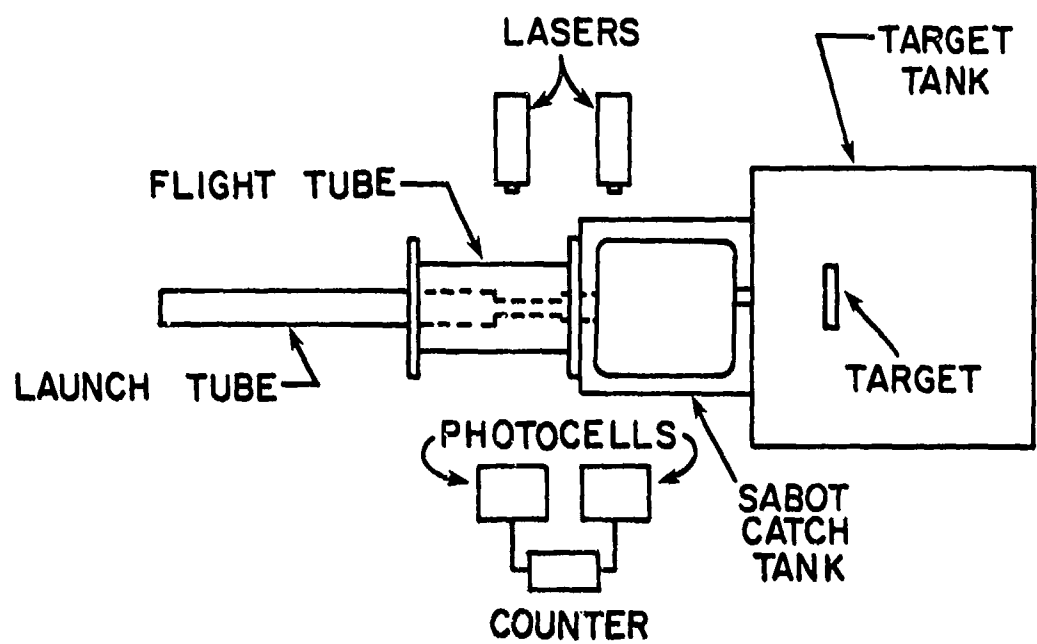
Figure 6. Schematic of Range Setup for Smaller Size
Projectile Impacts.

20

such as steel sphere and pebble impacts, the test specimens were
positioned in the sabot catch tank to permit locating the targets
as close as possible to the gun muzzle for shot accuracy purposes.
Since all of the impacts were to be leading edge hits, projectile
trajectory accuracy was critical. For the ice ball impacts, the
test specimens were positioned in the target tank.

Various smooth bore launch tubes were used on the
range depending on the size of the projectiles. The steel sphere
impacts were conducted on a launch tube having a bore of 7.62 mm
(30 cal) and a length of 0.91 m (3.0 feet). The pebble impacts
were conducted using launch tube having a bore of 12.7 mm (0.5
inches) and a length of 1.83 m (6.0 feet). The ice ball impacts
used a launch tube having a bore of 38.1 mm (1.5 inches) and a
length of 1.83 m (6.0 feet). In every case, the projectile was
fitted into a recessed pocket in a lexan sabot to provide protection
and support for the projectile during launch. The projectile/sabot
package was launched down the tube by utilizing either compressed
gas or powder gas depending on the desired impact velocity. Com-
pressed gas was used for impact velocities up to 305 m/s (1000 ft/s).
Above 305 m/s (1000 ft/s) a powder gun was used. A sabot stopper
device was located at the muzzle of the launch tube. The purpose
of this device was to slow down and eventually stop the sabot, per-
mitting the projectiles to separate from the sabot and continue on
trajectory towards the target specimen.

2.2.2   Large Bore Compressed Gas Gun Range

The range setup for the 85 g (3 ounce) artificial bird
and ice slab shots were conducted on a 51 mm (2.0 inch) smooth bore
gas gun having a length of 7.9 m (26.0 feet). The projectiles
were launched in a standard one-piece balsa wood sabot having a
cylindrical pocket. No attempt was made to stop the balsa wood
sabots because of the high velocities involved in the impacts. A
preslicer was used in conjunction with the launch tube to slice a
portion of the bird or ice projectile prior to impact such that
only the center portion of the bird diameter would actually load

21

the target specimen since the impacts were leading edge hits. In
the leading edge impacts, the specimens were positioned such that
slicing would occur; thus, only the center portion of the projectile
would load the specimens.

2.2.3 Mounting Procedure

All of the testing, except for a few, were conducted
using the free-free method of mounting by taping the specimen to a
mounting frame as shown in Figure 7. Upon impact, this free-free
method of mounting would permit the specimen to free flight.

One artificial bird impact was conducted with the
cantilever method of mounting by clamping one end of the test
specimen within a vise-like fixture. The vise-like fixture was
attached to the range beam in a manner that permitted proper align-
ment and orientation of the specimen with respect to the projectile
trajectory.

Four impacts were conducted with the specimens being
in a fixed-fixed method of mounting during the preload tests. The
preload tests fixture is described below.

Target alignment for an impact was achieved by pro-
jecting a laser beam through the bore of the launch tube onto the
desired impact site of the target. For the case of edge impacts
by the small hard projectiles, the target was positioned such that
the laser beam was split by the target edge at the desired impact
site.

2.2.4 Preload Tests

The effects of preload (centrifugal loading in a blade)
was investigated. The apparatus utilized to preload specimens is
shown in Figure 8. It consisted of a beam supported by a structure
such that a 30 to 1 moment arm exists. By attaching the specimen at
one end of the beam and placing weight to the other end, the specimen
could be loaded in tension. By knowing the moment arm and weights
accurately, the amount of force applied to the specimen was calculated.
The cross-sectional area of the specimen was known, therefore, the
stress could be calculated in the preload testing for the specimens.

22
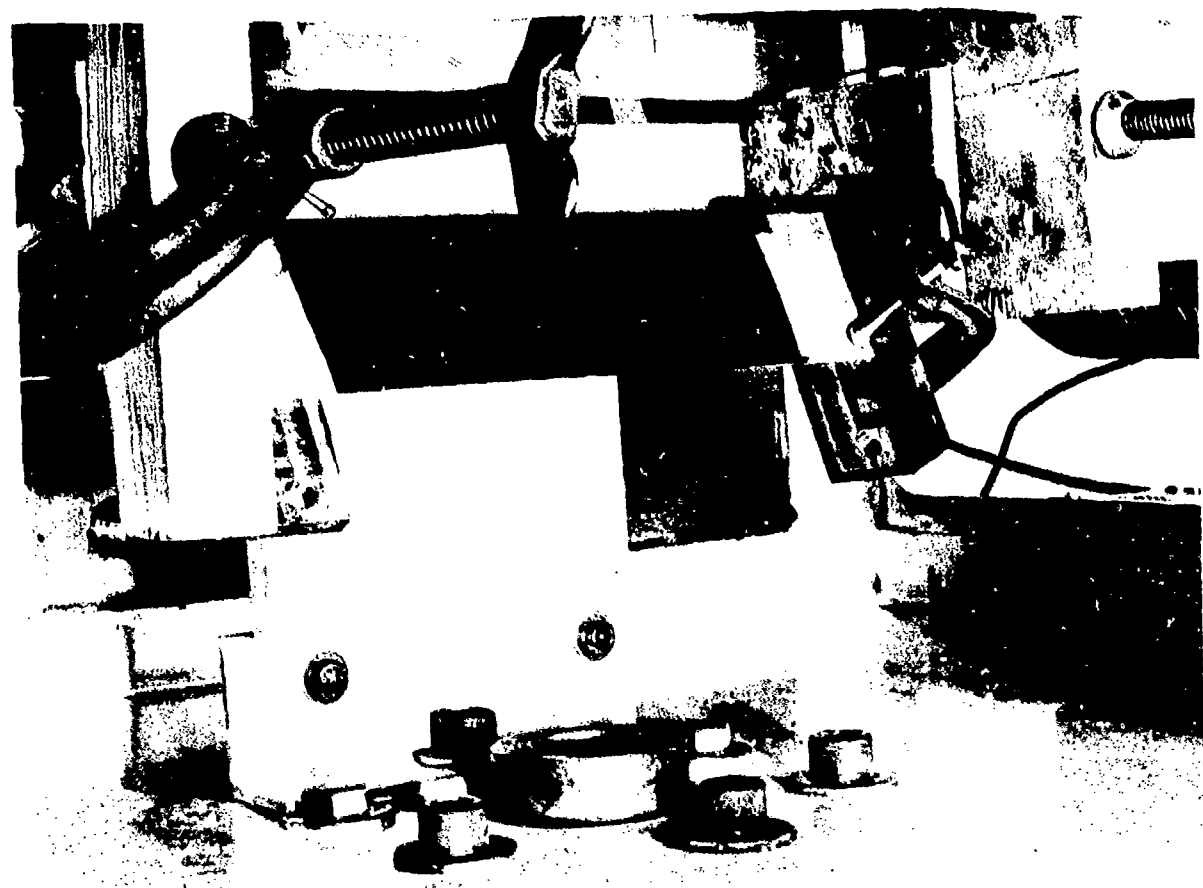
Figure 7.   Mounting Frame for Free-Free Method of Mounting.

23
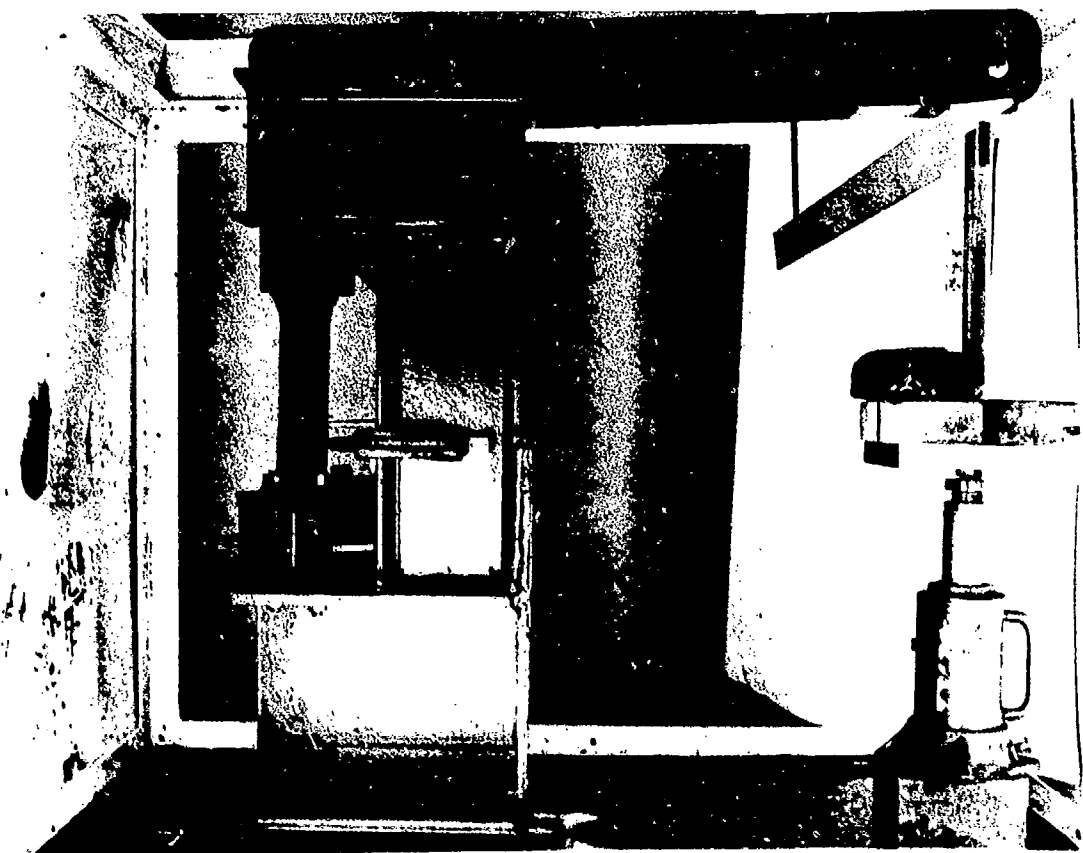
Figure 8. Apparatus Utilized to Preload Specimens.

2.2.5   Slice Size Determination

The mass of the projectile which actually impacts
the specimen was of great importance in the leading edge impacts.
The most satisfactory technique for determining the impact mass
involved recovering the presliced portion and the nondeflected
portion (slice across leading edge of the specimen) and accurately
weighing them. The mass recovered was then subtracted from the
initial mass of the projectile to provide a realiable and accurate
value for the impact slice mass.

2.2.6   Impact Velocity Measurements

The projectile velocity for the large compressed gas
gun was measured by utilizing a pair of HeNe laser/photomultiplier
stations spaced a known distance apart. Each laser projects a
beam that intersects the projectile trajectory normal to trajectory
and illuminates one of the photomultiplier stations. When the pro-
jectile interrupts the first beam, the first photomultiplier station
generates a voltage pulse to start a countertimer and trigger a
light source for a still camera. The countertimer is stopped and
the other light source is triggered when the projectile interrupts
the second laser beam. The projectile impact velocity was then
calculated from the recorded measured time and the distance traveled.
This technique provided accurate velocity measurements and data on
projectile integrity just prior to impact. The smaller bore FOD
gun range utilized a similar technique except that still photographs
of the projectile in flight were not taken.

2.3   DAMAGE ASSESSMENT

The damage assessment portion of the data collected was given
particular consideration in the study. The mode of damage was deter-
mined and the extend of damage measured. It was anticipated that
tests would be conducted on the damaged specimens to determine the
residual tensile strength and residual fatigue strength properties;
however, none of the specimens displayed damage where the residual
tensile strength would be affected to any extent. In the case of

the residual fatigue strength properties, the damage on the specimens was in the form of bulges and mass loss modes without any tearing at the impact site. The test conditions were such that the impact velocities for the particular blade types were not at critical values where a bulge with a tear results. Previous testing had demonstrated that the extend of fatigue damage depends primarily on the type of damage and appears to be relatively independent of size of damage. (Reference 5). The least severe fatigue damage was demonstrated for impacted leading edges to be clean perforations with complete material removal. The next worse case was that where the leading edge curled back extensively or bulged. The worst case was demonstrated to be where the curl back or bulge initiated a rip or tear along the leading edge from which the fatigue crack could propagate. Because of the physical size of the specimens (87 to 290 mm^2 cross-sectional area depending on the blade type) and the minimal damage received from the impacts, the tests to determine the residual fatigue strength were deleted. Testing of the fatigue properties of the composite materials in the Task IV C phase of the program also indicated that the composite materials were insensitive to fatigue which is another reason for deleting the fatigue tests.

2.3.1   Mode and Extent of Damage Measurements

The foreign object damage (FOD) problem can be divided into two separate areas, both of which are associated with a damage threshold. One deals with local blade damage; the other is associated with large scale structural damage. It was the purpose of this subtask to investigate the local damage problem area.

The damage modes occurring on the metal specimens due to leading edge FOD impact depended on the type of impactor (small and hard or large and soft). The damage mode for the small hard impactors such as the glass beads and chrome steel spheres was a leading edge dimple or bulge or mass loss. A typical dimple or bulge damage mode on the leading edge is shown in Figure 9. A typical damage mode of mass loss from the leading edge is shown in Figure 10. In the case of large soft impactors on the metal specimens, the damage mode was in the form of plastic deformation without cracking

26

3-0063
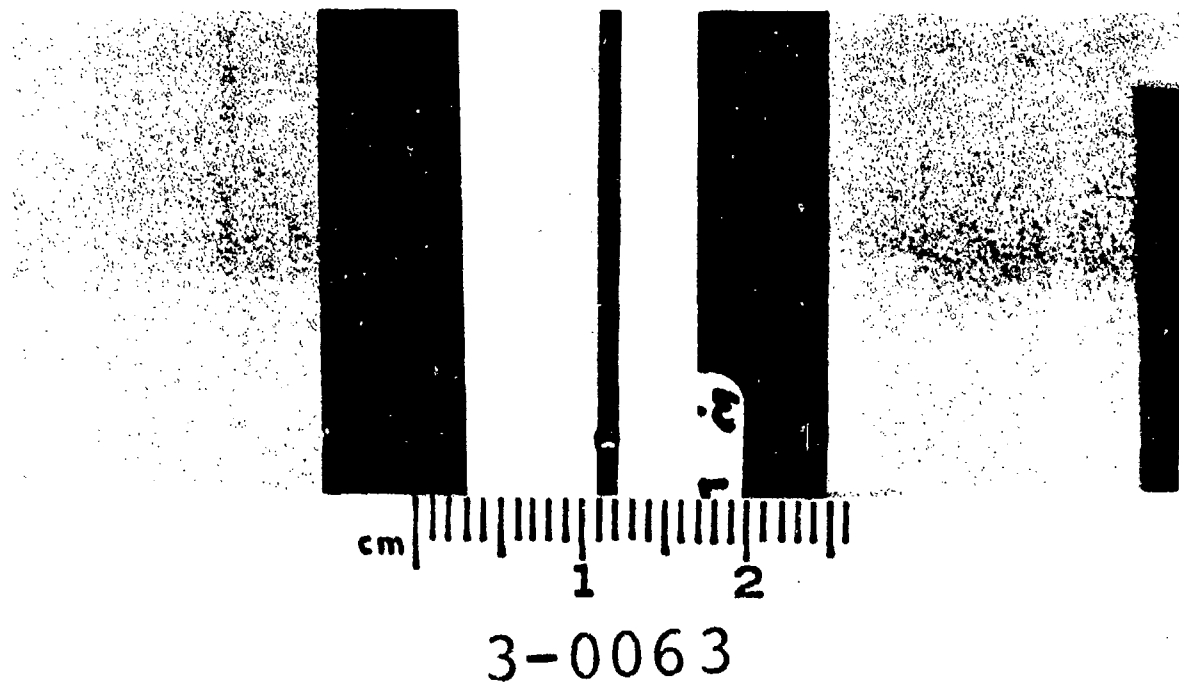
Figure 9.   Typical Dimple or Bulge Type Damage Mode on Specimen
            Leading Edge.

27
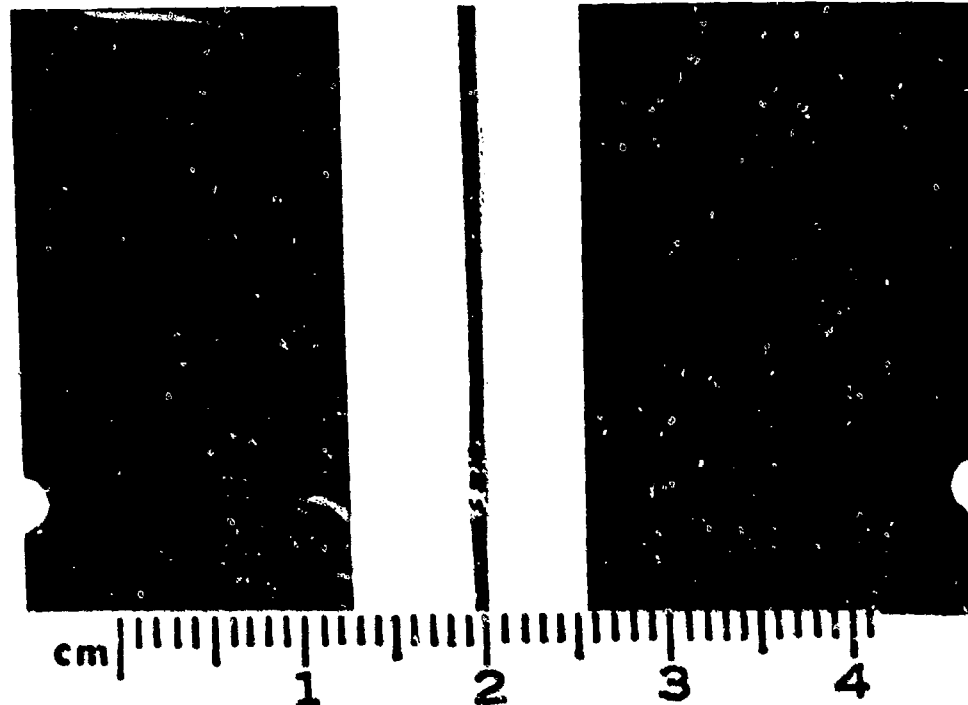
3-0220

Figure 10.   Typical Mass Loss Type Damage Mode on Specimen
Leading Edge.

or curlback or a large amount of local bending at the impact site. In some cases, the local bending was extensive by deforming the specimen into a horseshoe shape as shown in Figure 11.

The dimple bulge or mass loss damage modes were characterized by making width, depth, and maximum deformation (plastic) measurements of the leading edge damage on the specimens. The width measurement corresponds with the span direction of the specimens and the depth measurement with the specimen chord direction.

In the case of large soft body and pebble impacts, the damage was characterized by measuring the maximum plastic deformation of the specimen leading edge (L.E.) and trailing edge (T.E.) where possible. Twist of the specimen in the span direction was also measured where specimens encountered twist damage. When the damage was substantial such as bending the specimen into a horseshoe shape, the damage was described but not measured. Photographs of all the impact damage were also taken.

The boron/aluminum composite specimens had similar damage to the metal specimens for the small hard impactors since all of the composite specimens had nickel plating on its leading edge. Again, this damage was characterized by giving the width, depth and maximum plastic deformation measurements of the leading edge damage.

Figure 11.   Extensive Bending Damage Mode at Impact Site.

SECTION III
EXPERIMENTAL RESULTS

The experimental results of the specimen leading-edge impact study to investigate local damage are summarized in the following paragraphs. A total of 128 data shots consisting of Pyrex or glass sphere, chrome steel sphere, pebble, ice ball, and artificial bird impacts were conducted on the three materials investigated. Tables of all the impacts giving the test conditions, damage measurements, and a description of the damage are presented in the Appendix.

3.1 PYREX AND GLASS BEAD IMPACTS

The first table of the Appendix gives the results of 0.79, 1.59, and 3.18 mm diameter Pyrex or glass bead impacts conducted on either 403 stainless steel specimens, a F101 blade or an APSI blade. In all cases, only slight damage resulted from the leading edge impacts with the projectiles breaking up upon impact. To avoid the uncertainty surrounding the effect of projectile break-up upon the damage inflicted on the test specimens and actual blades, chrome steel spheres were substituted for the glass bead. Typical damage received for Pyrex or glass sphere impacts on the three materials investigated are shown in Figures 12 through 14.

3.2 CHROME STEEL SPHERE IMPACTS

A preliminary series of tests indicated that minimal damage was received from the 0.76 mm (30 mil) chrome steel impacts. In order to obtain meaningful data, the size of the chrome steel spheres was increased to 1.59 and 3.18 mm (60 and 125 mil) diameter to receive measureable damage from the leading edge impacts. Table 7 presents a summary of the damage results for the various specimen types and projectile sizes. Impacts at similar test conditions are grouped together and averaged. The number in parenthesis in the table indicates the number of tests (impactor type, size, and velocity) in that group.

31

Table 7. Summation of Chrome Steel Sphere Impacts

Specimen Type	Specimen Overall Leading Edge Thickness (mm)	Specimen Nickel Plating Thickness (mm)	Projectile Size (mm)	Impact Velocity (m/s)	Impact Angle (°)	Damage Width (mm)	Depth (mm)	Maximum Plastic Deformation (mm)
403SS(7)	1.22	--	1.59	251	36.4	1.14	0.10	0.09
403SS(5)	1.22	--	3.18	240	36.4	2.27	0.66	0.64
410SS(5)	0.61	--	1.59	242	36.4	1.37	0.32	0.45
403SS(5)	1.22	--	1.59	168	51.1	1.24	0.17	0.00
403SS(6)	1.22	--	3.18	180	51.1	2.58	0.48	0.37
410SS(5)	0.61	--	1.59	174	51.1	1.22	0.25	0.26
8-1-1 Ti(6)	0.81	--	1.59	386	24.4	1.45	0.54	--
8-1-1 Ti(5)	0.81	--	3.18	393	24.4	3.18	1.75	--
8-1-1 Ti(5)	0.81	--	1.59	308	41.0	1.60	0.45	--
8-1-1 Ti(6)	0.81	--	3.18	310	41.0	3.27	1.18	--
B/Al(5)	1.22	0.58	1.59	434	18.9	1.30	0.98	0.08
B/Al(5)	1.30	0.64	3.18	418	18.9	2.18	2.40	0.51
B/Al(5)	0.97	0.32	1.59	439	18.9	0.97	1.02	0.19

Note: Number in parenthesis indicates number of tests conducted in that group.

32
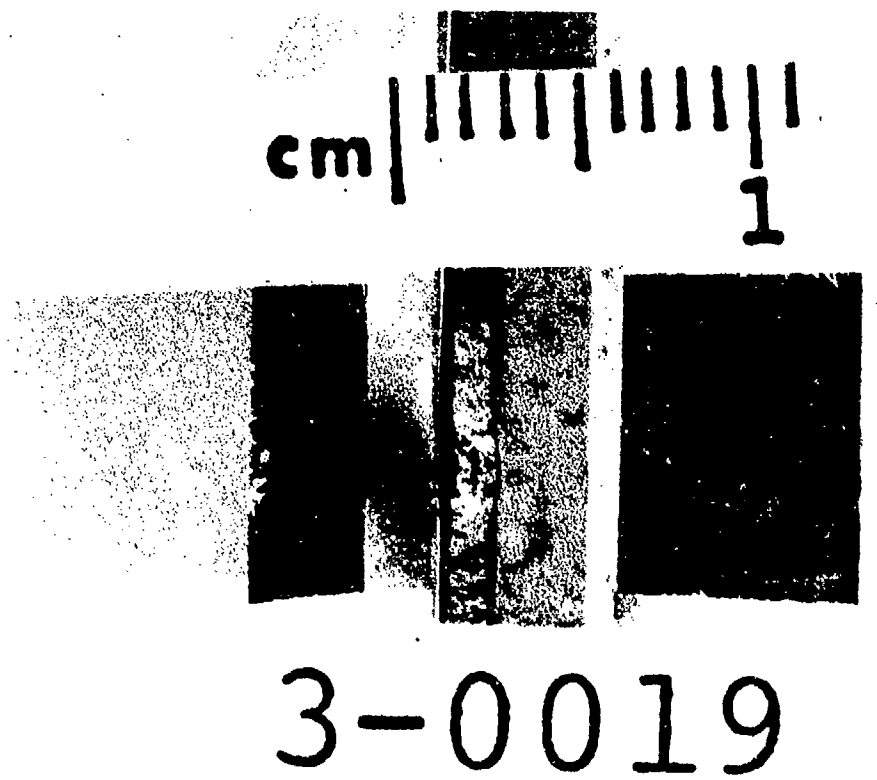
Figure 12.   Typical Damage Received on 403 Stainless Steel
             Specimen from 3.18 mm Diameter Pyrex Sphere
             Impact.
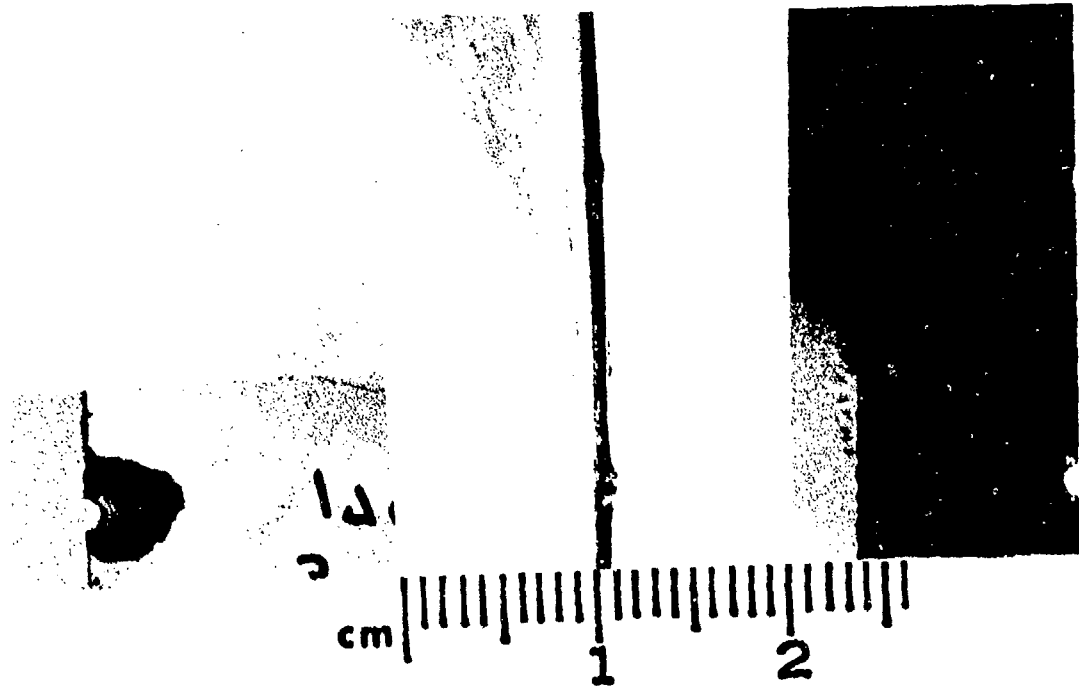
Figure 13. Typical Damage Received on F101 Blade from 3.18 mm Diameter Pyrex Sphere Impact.
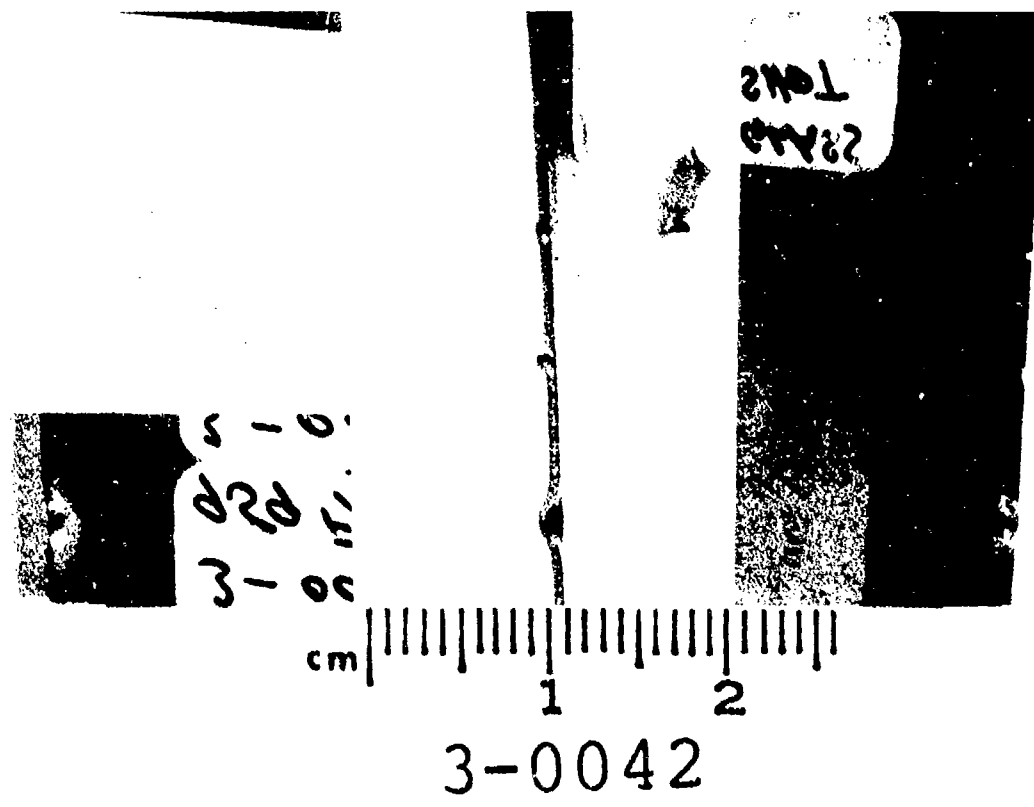
Figure 14.   Typical Damage Received on APSI Blade from 3.18 mm
             Diameter Pyrex Sphere Impact.

3.2.1　Results of Stainless Steel Specimens

A series of impact tests was conducted on stainless steel specimens using 1.59 and 3.18 mm diameter chrome steel spheres as the impactors. Tests were conducted on two different leading edge thickness type specimens to determine if geometric scaling is linear in impact events. One leading edge thickness was 1.22 mm using specimens of 403 stainless steel material and the other thickness was 0.61 mm using specimens of 410 stainless steel material. The impacts were leading edge impacts at two angles of incidence of 36.4 and 51.1 degrees at impact velocities of about 240 and 170 m/s, respectively. Both sizes of spheres were utilized on the thicker leading edge specimen impact tests while only 1.59 mm diameter sphere impacts were conducted on the 0.61 mm leading edge thickness specimens.

The type of damage received for the impacts was in the form of a dent or dimple with a bulge. No cracks or tearings were observed at the impact site which indicates that the impact velocities were below critical values where a bulge with a tear results. Previous testing has demonstrated that the extent of fatigue damage depends primarily on the type of damage and appears to be relatively independent of size of damage (Reference 5). The worse case was demonstrated to be where the curl back or bulge initiated a rip along the leading edge from which the fatigue crack could propogate. The next worse case for fatigue was where the leading edge curled back extensively or bulged. The least severe fatigue damage for impacted leading edges was a clean perforation with complete material removal. Based on these results, it is evident that the impact velocity to generate the worse case of a bulge with a rip or tear had to be much higher than was utilized. Based on these results and the minimal damage received from the impacts in this series of tests, the tests to determine the residual fatigue strength properties were deleted.

A summary of the damage results for the stainless steel specimen impacts is given in Table 7. Plots of the measured

36

damage values versus the impact velocity are given in Figure 15
through 17. Figure 15 gives a plot of the measured average nick
width damage while Figure 16 shows a plot of the measured average
nick depth damage. Figure 17 presents a plot of the maximum plastic
deformation versus the impact velocity. The damage received in the
study for the impacts were very similar in appearance for the two
leading edge thicknesses; the damage values for the plastic de-
formation should scale lineraly and be geometrically identical as
long as wave propagation and resulting inertia effects are not im-
portant. One would expect that the damage in a 0.61 mm thick spec-
imen due to an impact of a 1.59 mm projectile would be one-half
the values to that in a 1.22 mm thick specimen impacted with a 3.18
mm projectile.

For the 36.4 degree impacts at the same velocity, the
1.22 mm thick specimens had damage values of 2.27 mm for the width,
0.66 mm for the depth, and 0.64 mm for the plastic deformation.
For identical test conditions, the 0.61 mm thick specimens had
damage values of 1.37 mm for the width, 0.32 mm for the depth, and
0.45 mm for the plastic deformation.

It is felt that the width and depth measurements are
due to the footprint of the sphere projectiles and are probably
secondary in importance. The plastic deformation damage is the
important damage parameter to consider when investigating scaling.
In determining if geometric scaling concepts are applicable, the
damage for these specimens is about 20 percent too high for the
width measurement, 3 percent too low for the depth measurement, and
41 percent too high for the plastic deformation measurement. Thus,
linear scaling is fairly good for the width, excellent for the
depth, and fair for the plastic deformation.

For the 51.1 degree impacts at similar velocities,
the 1.22 mm thick specimens had damage values of 2.58 mm for the
width, 0.48 for the depth, and 0.37 mm for the plastic deformation.
The 0.61 mm thick specimens had damage values of 1.22 mm for the
width, 0.25 mm for the depth, and 0.26 mm for the plastic deformation.
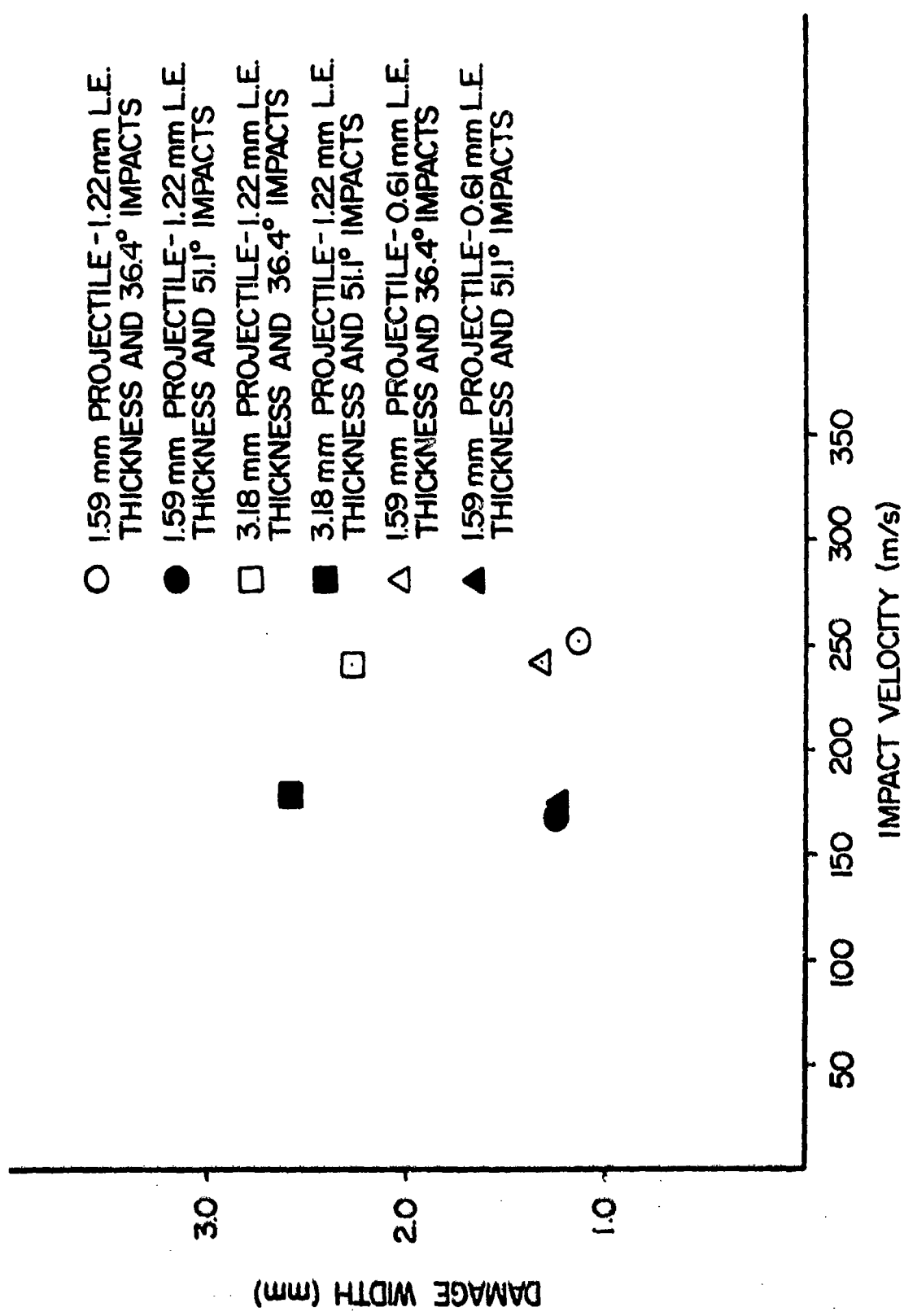
Figure 15. Plot of Damage Width Versus Impact Velocity for Stainless Steel Specimens.
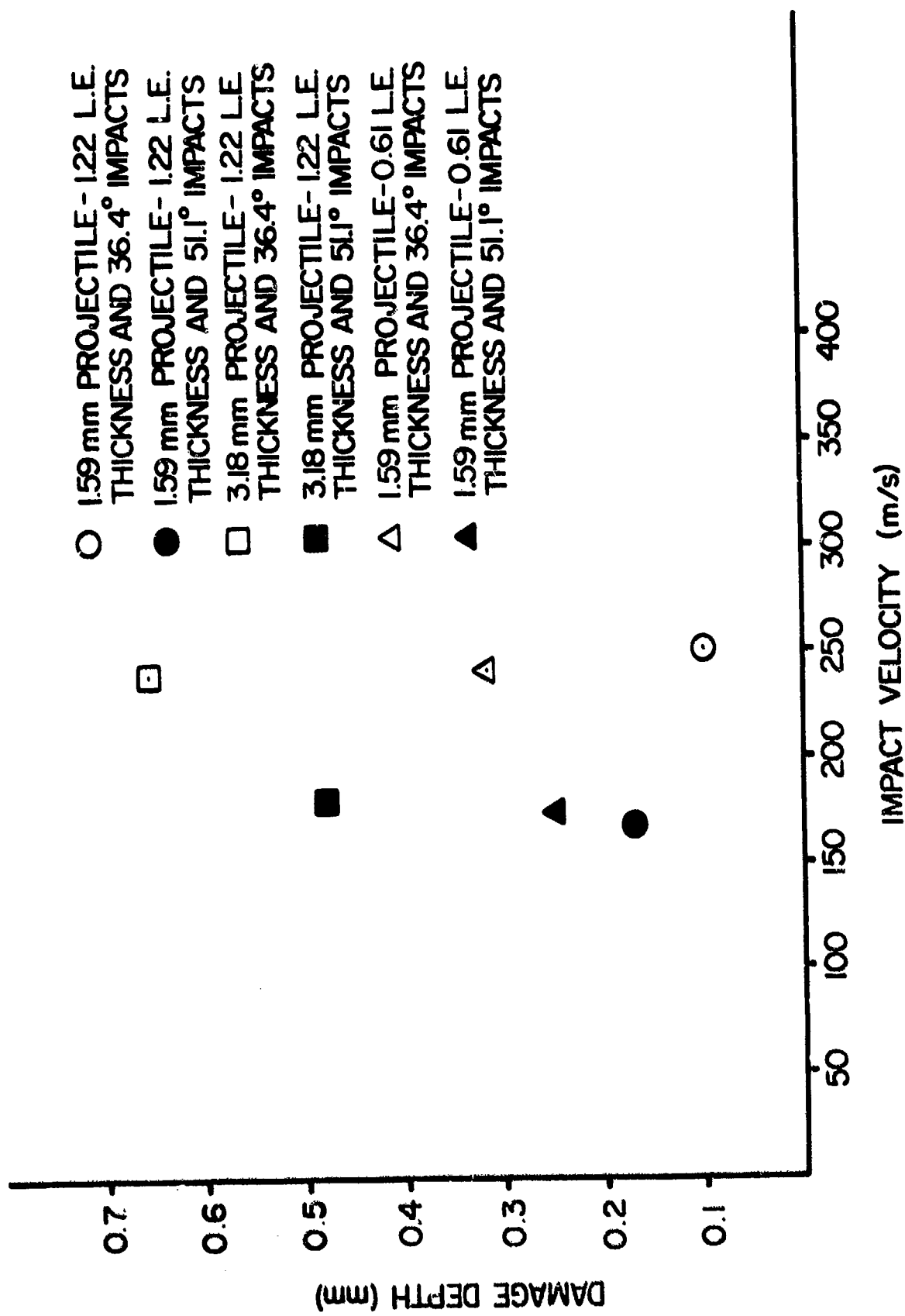
Figure 16. Plot of Damage Depth Versus Impact Velocity for Stainless Steel Specimens.
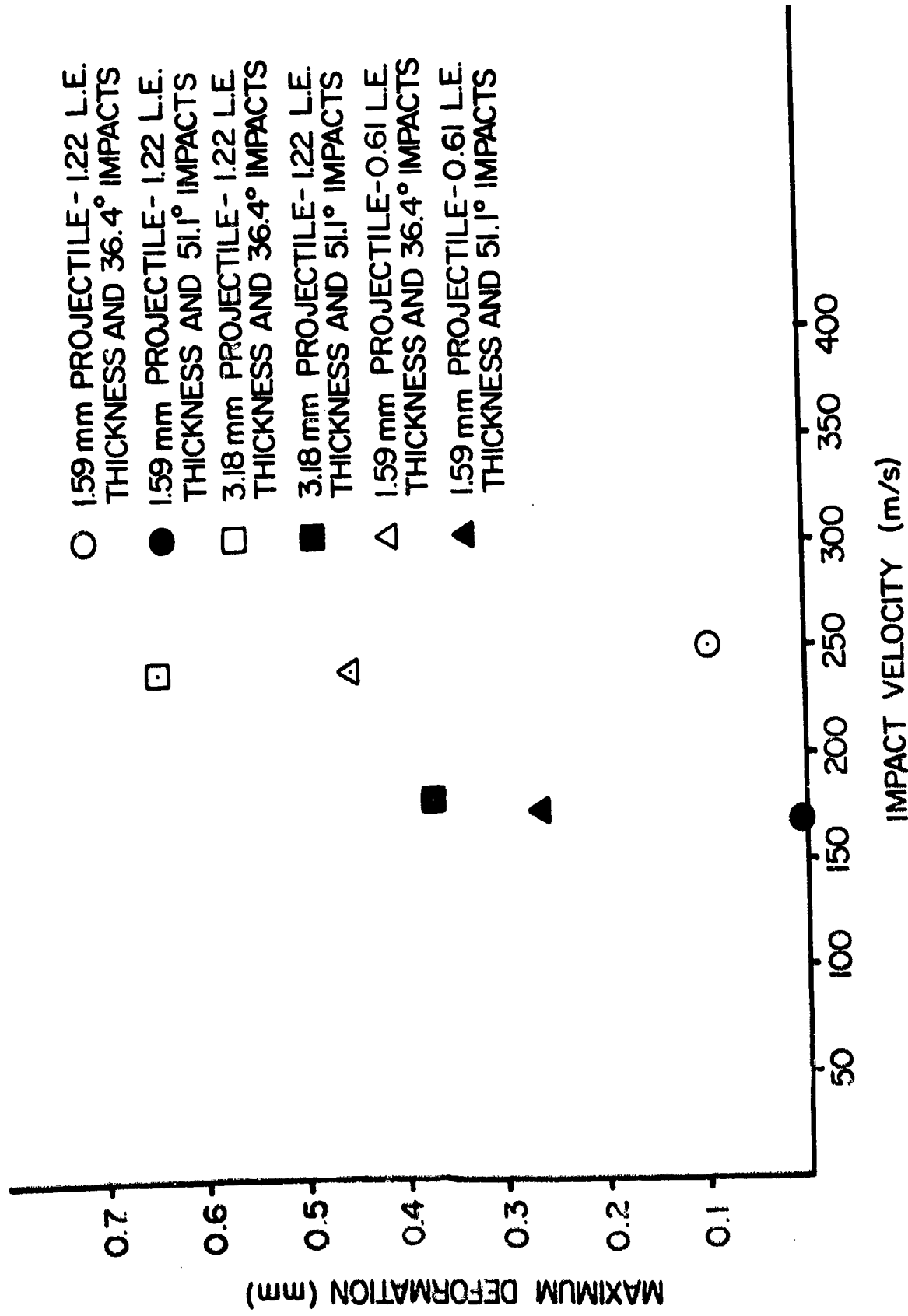
Figure 17. Plot of Maximum Plastic Deformation Damage Versus Impact Velocity for Stainless Steel Specimens.

40

Based on these measurements, the damage for the thin specimens is about 5 percent too low for the width measurement, 4 percent too high for the depth measurement, and 41 percent too high for the plastic deformation. Thus, linear scaling for this group is excellent for the width and depth measurements and fair for the plastic deformation.

The damage was similar in appearance for all cases; however, the concept of geometric scaling did not seem to work as well as expected. The scaling seemed to be fairly good for the width and depth damage and fair for the maximum deformation damage.

Typical damage on the six stainless steel group impacts is shown in Figures 18 through 23.

3.2.2 Results of Titanium Specimens

A series of leading edge impact tests was conducted on 8-1-1 titanium specimens using 1.59 and 3.18 mm diameter chrome steel spheres as the impactors. The tests were conducted on a specimen leading edge thickness of 0.81 mm at angles of incidence of 24.4 and 41.0 degrees at velocities of approximately 390 and 310 m/s, respectively.

The type of damage received for the impacts was in the form of mass loss from the specimen leading edge which indicates that the impact velocities were above the critical velocity value where a bulge with a rip or tear occurs.

A summary of the damage results given in Table 7 for the titanium specimen impacts indicates that the damage is somewhat greater for the 41.0 degree impacts at a lower velocity than for the 24.1 degree impacts. Plots of the measured damage values versus the impact velocity are given in Figures 24 and 25. Figure 24 gives a plot of the average damage width while Figure 25 shows the average damage depth. In the case of the titanium impacts there was negigible plastic deformation on the specimens.

Typical damage for the titanium impacts is shown in Figures 26 and 27 for the different size projectiles.

41

Figure 18. Typical Damage Received on 1.22 mm L.E. Thickness
Stainless Steel Specimens from 1.59 mm Projectile
Impacts at 36.4°.
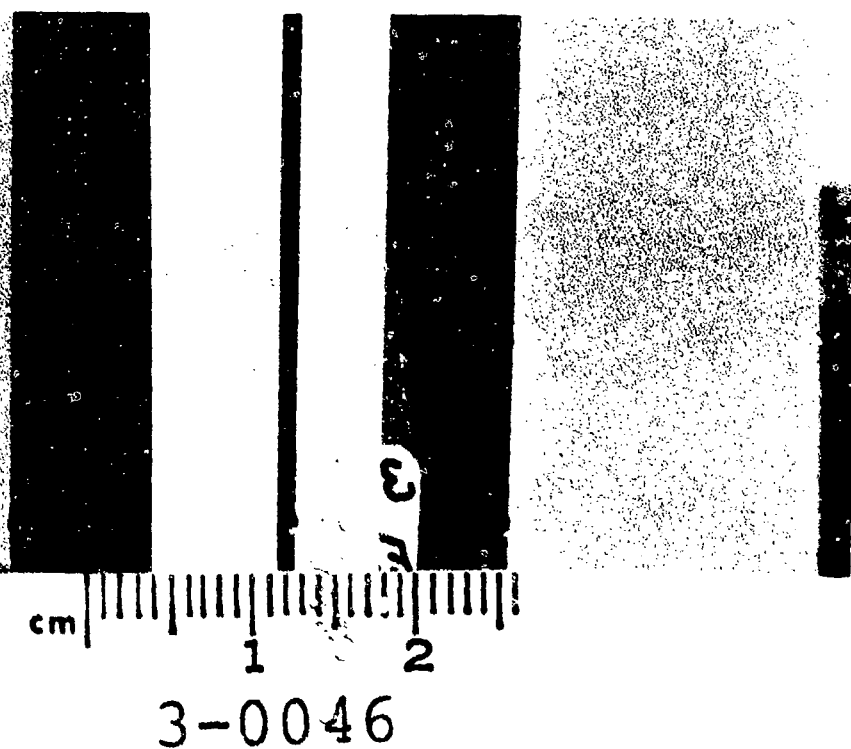
Figure 19. Typical Damage Received on 1.22 mm L.E. Thickness
Stainless Steel Specimens from 1.59 mm Projectile
Impacts at 51.1°.

3-0067
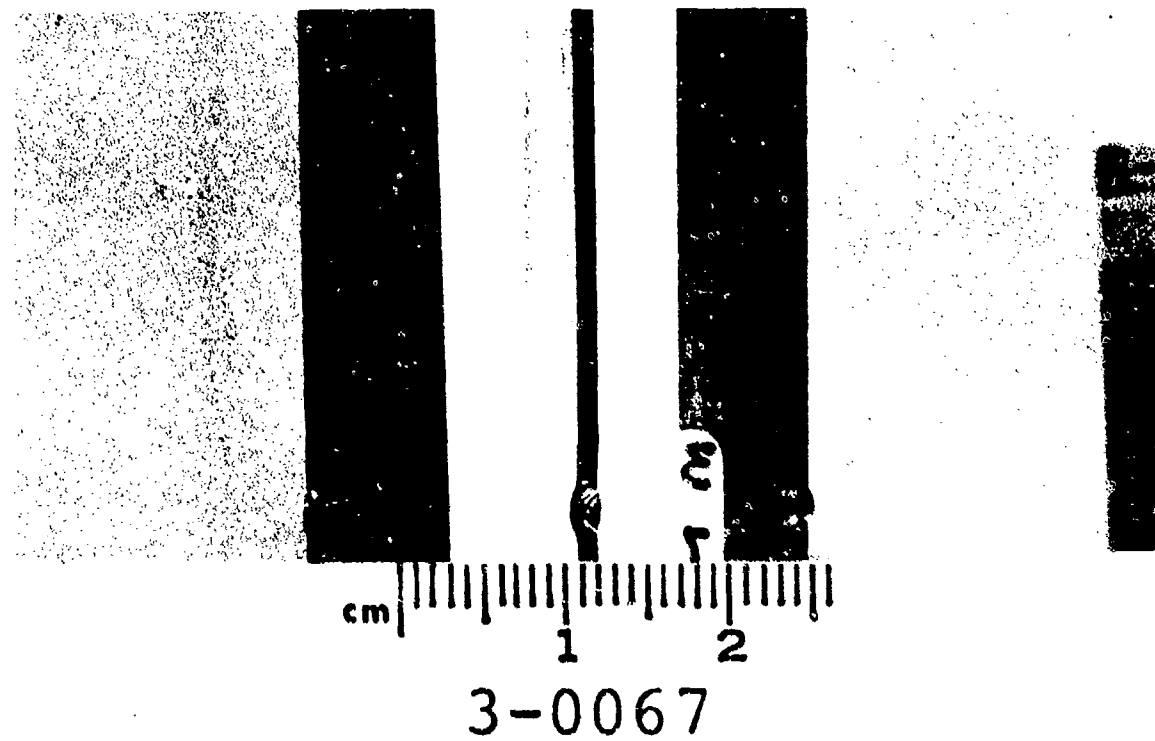
Figure 20.   Typical Damage Received on 1.22 mm L.E. Thickness
              Stainless Steel Specimens from 3.18 mm Projectile
              Impacts at 36.4°.

44

3-0052
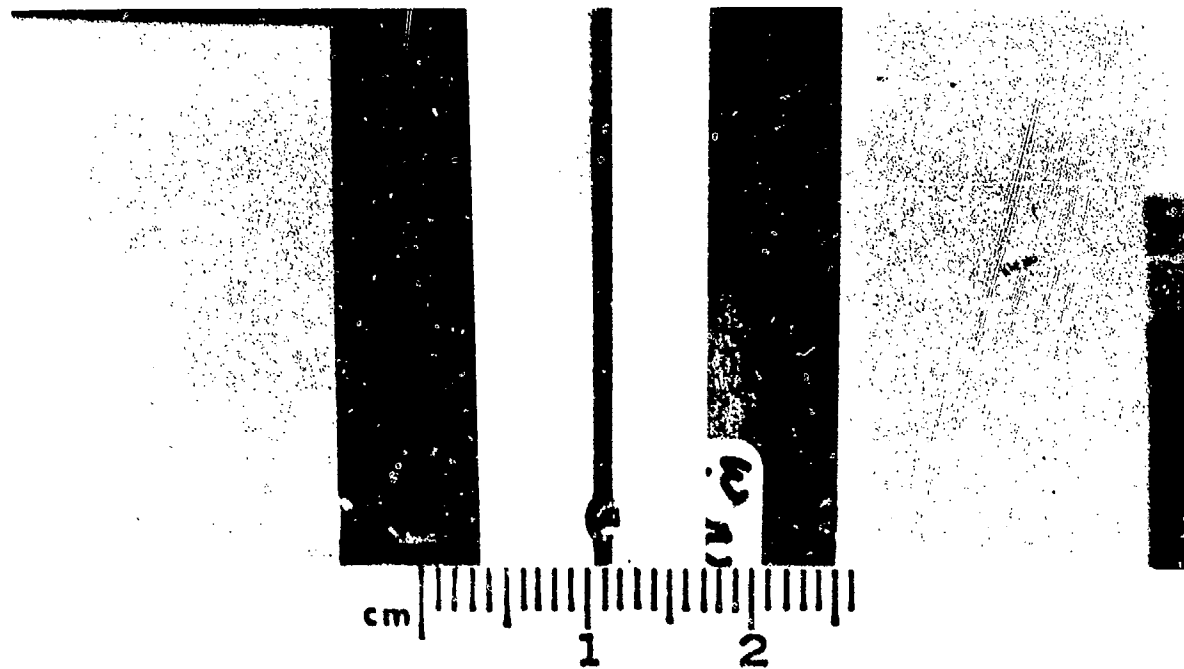
Figure 21. Typical Damage Received on 1.22 mm L.E. Thickness
Stainless Steel Specimens from 3.18 mm Projectile
Impacts at 51.1°.
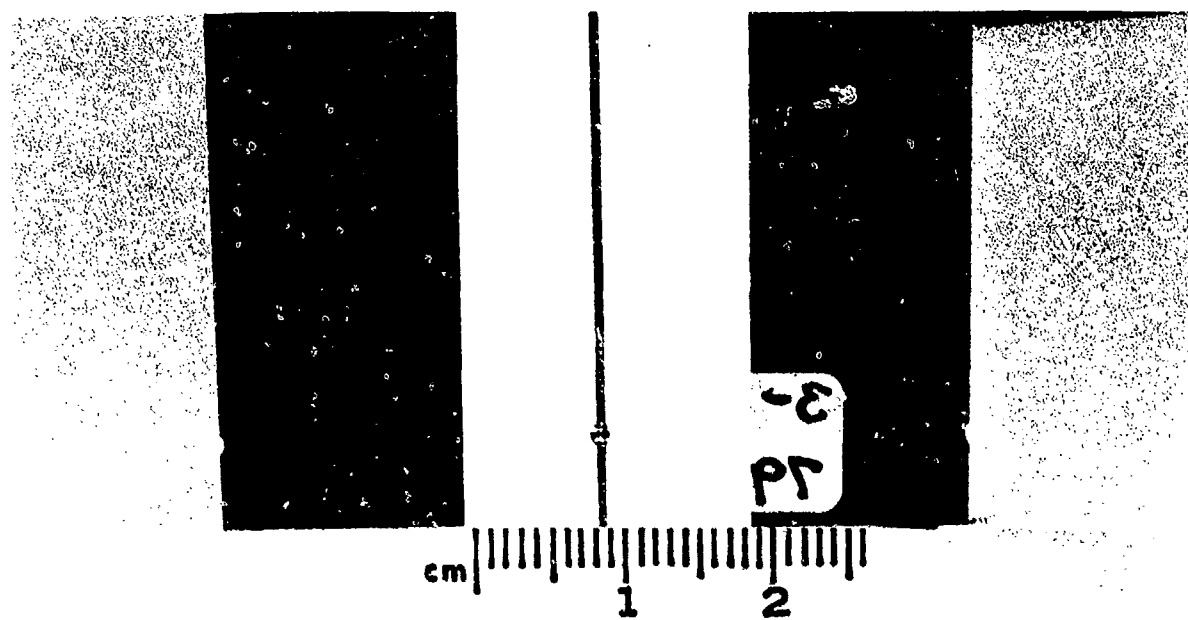
Figure 22.   Typical Damage Received on 0.61 mm L.E. Thickness Stainless Steel Specimens from 1.59 mm Projectile Impacts at 36.4°.
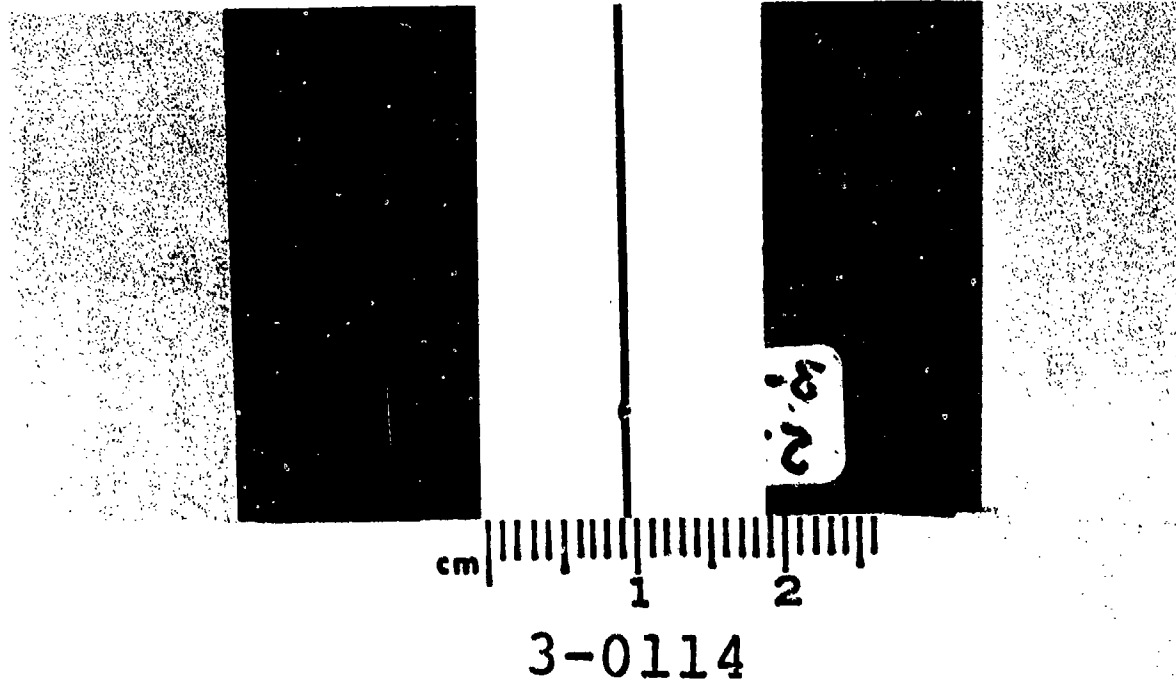
Figure 23. Typical Damage Received on 0.61 mm L.E. Thickness
Stainless Steel Specimens from 1.59 mm Projectile
Impacts at 51.1°.
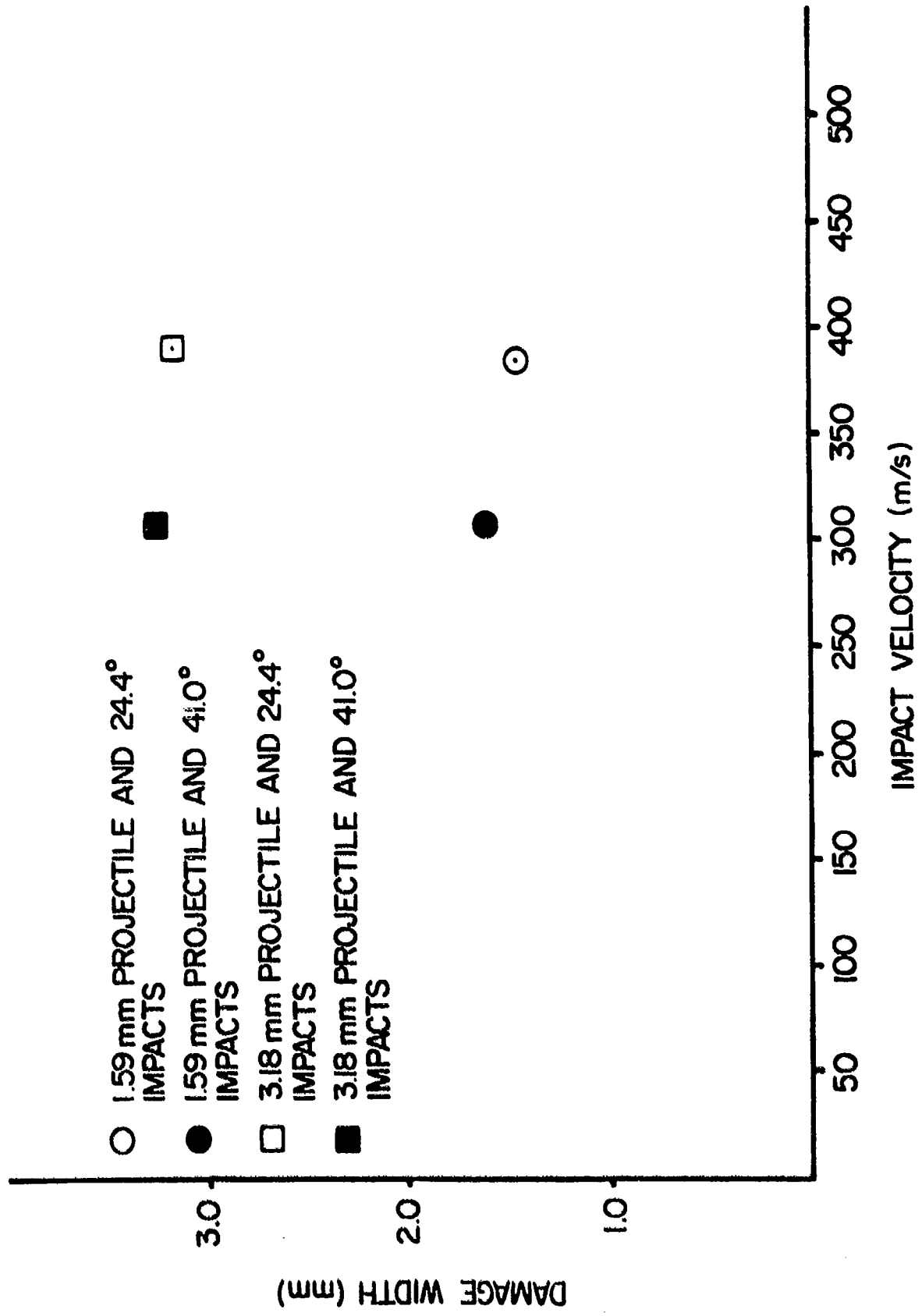
Figure 24. Plot of Damage Width Versus Impact Velocity for Titanium Specimens.

48
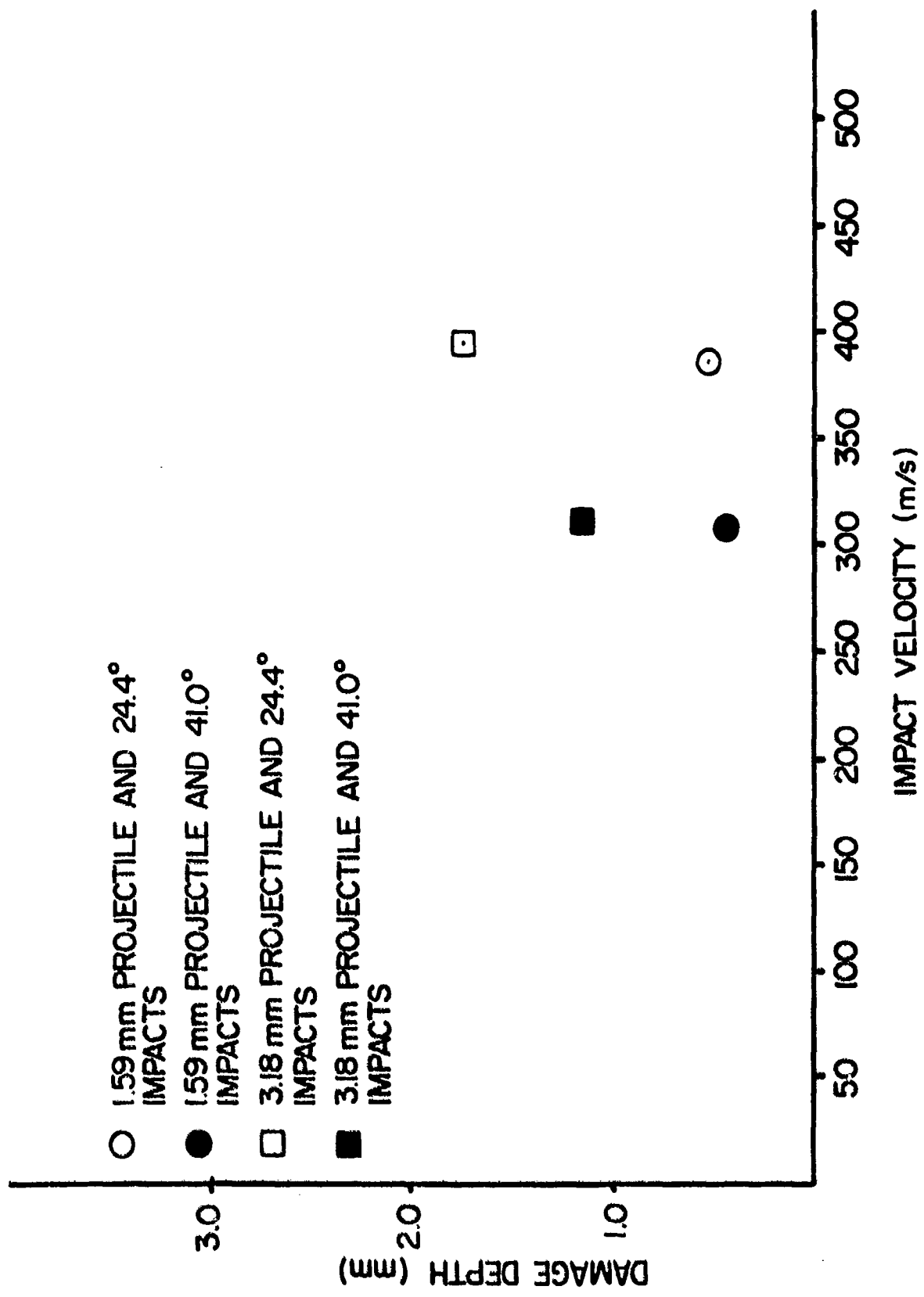
Figure 25. Plot of Damage Depth Versus Impact Velocity for Titanium Specimens.

49

cm

1   2   3   4
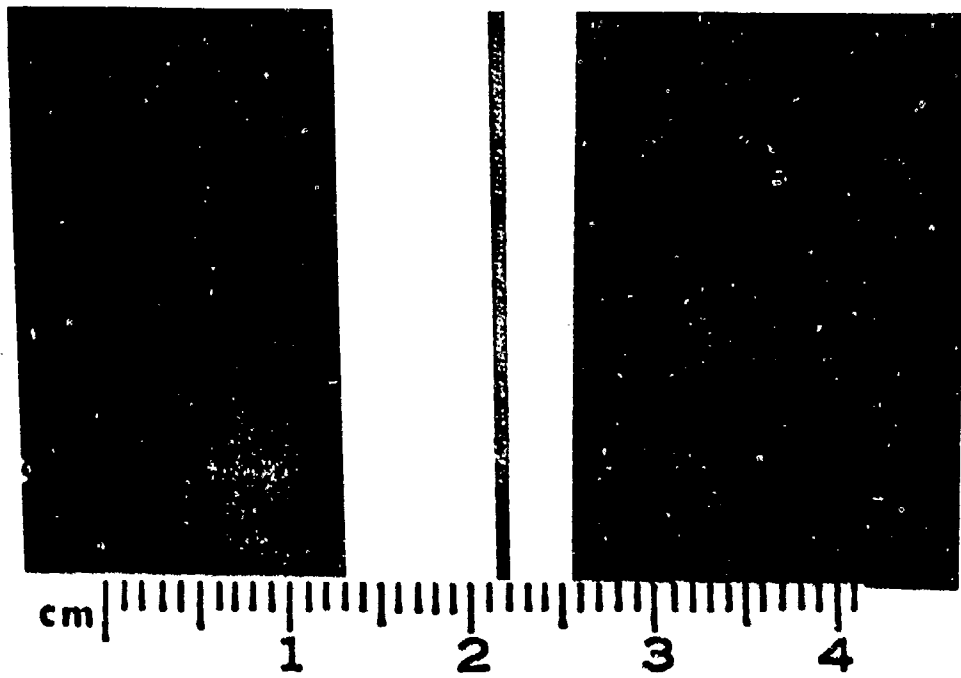
3-0234

Figure 26.   Typical Damage Received on Titanium Specimens from 1.59 mm Projectile Impacts at 24.4°.
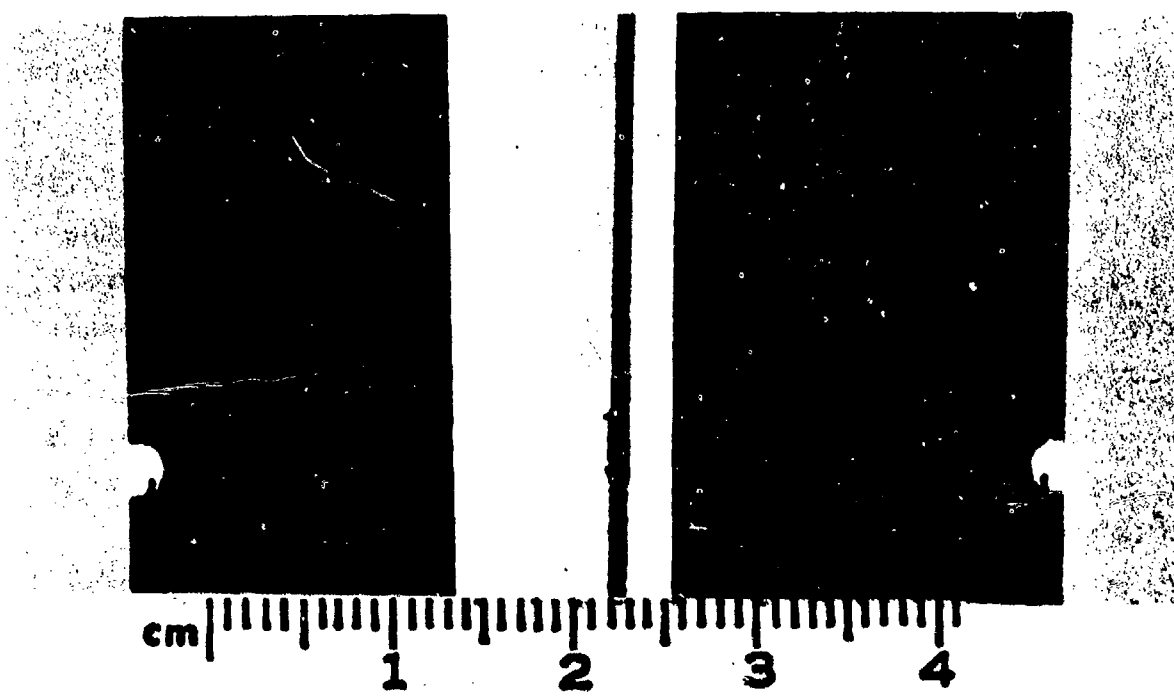
3-0239

Figure 27.   Typical Damage Received on Titanium Specimens
from 3.18 mm Projectile Impacts at 24.4°.

3.2.3   Results of Boron/Aluminum Specimens

A series of leading edge impact tests was conducted on boron/aluminum specimens with nickel leading edge protection using both 1.59 and 3.18 mm diameter chrome steel spheres as the impactors. Two different leading edge thickness specimen types were investigated to determine the damage response at an angle of incidence of 18.9 degrees. The impact velocity used in the tests was approximately 430 m/s.

The type of damage received was in the form of nicks with very little bulging. In some cases, the outer skin of the nickel leading edge protection material was rolled back; however, there were no rips or tears generated which indicates the impact velocity was below the critical velocity value.

A summary of the damage results given in Table 7 for the boron/aluminum impacts indicates that the impact velocity of 430 m/s with 1.59 mm projectiles will generate approximately similar damage values on both leading edge thickness specimens. Plots of the measured damage values versus the impact velocity are given in Figures 28 through 30. Figure 28 gives a plot of the average nick width while Figure 29 is a plot of the average nick depth. Figure 30 presents a plot of the average maximum plastic deformation damage versus the impact velocity for the composite specimens.

One reason that linear scaling may not work in the study for the composite material was that the overall thickness of the leading edge of the nominal and half-scale specimens were very much alike. Also, for accurate scaling, the wire size for the half scale specimens should have been half the diameter than that used in the nominal thickness specimens. The average overall leading edge thickness for the nominal thickness specimens was 1.22 mm for the 1.59 mm sphere impacts and 1.30 mm for the 3.18 mm impacts. The average overall leading edge thickness for the half scale specimens was 0.97 mm for the 1.59 mm sphere impacts. Thus, this variation in the overall thickness of the leading edge would have a considerable effect on the scaling of the damage.
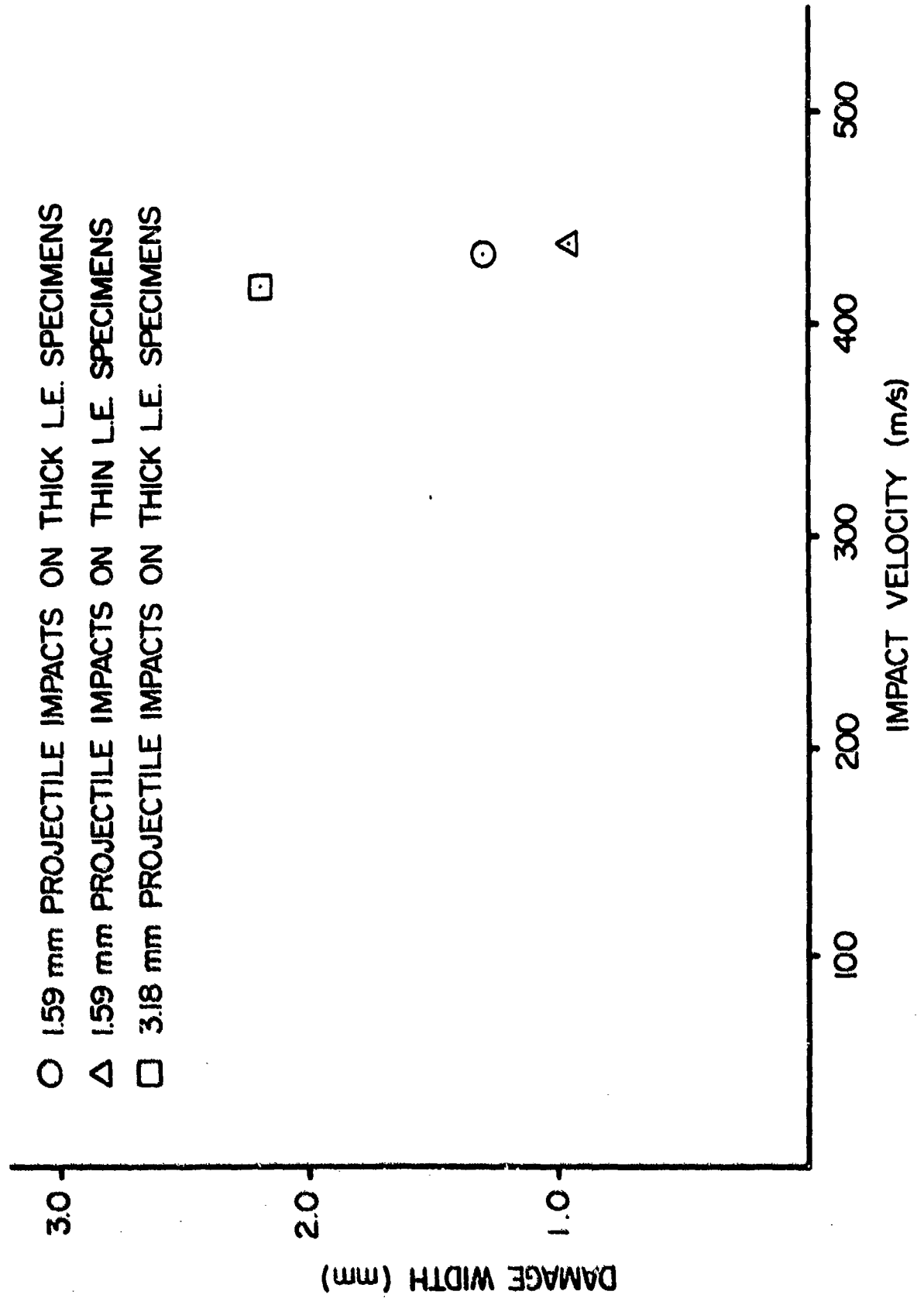
Figure 28. Plot of Damage Width Versus Impact Velocity for Boron/Aluminum Specimens.

O 1.59 mm PROJECTILE IMPACTS ON THICK L.E. SPECIMENS

△ 1.59 mm PROJECTILE IMPACTS ON THIN L.E. SPECIMENS

☐ 3.18 mm PROJECTILE IMPACTS ON THICK L.E. SPECIMENS
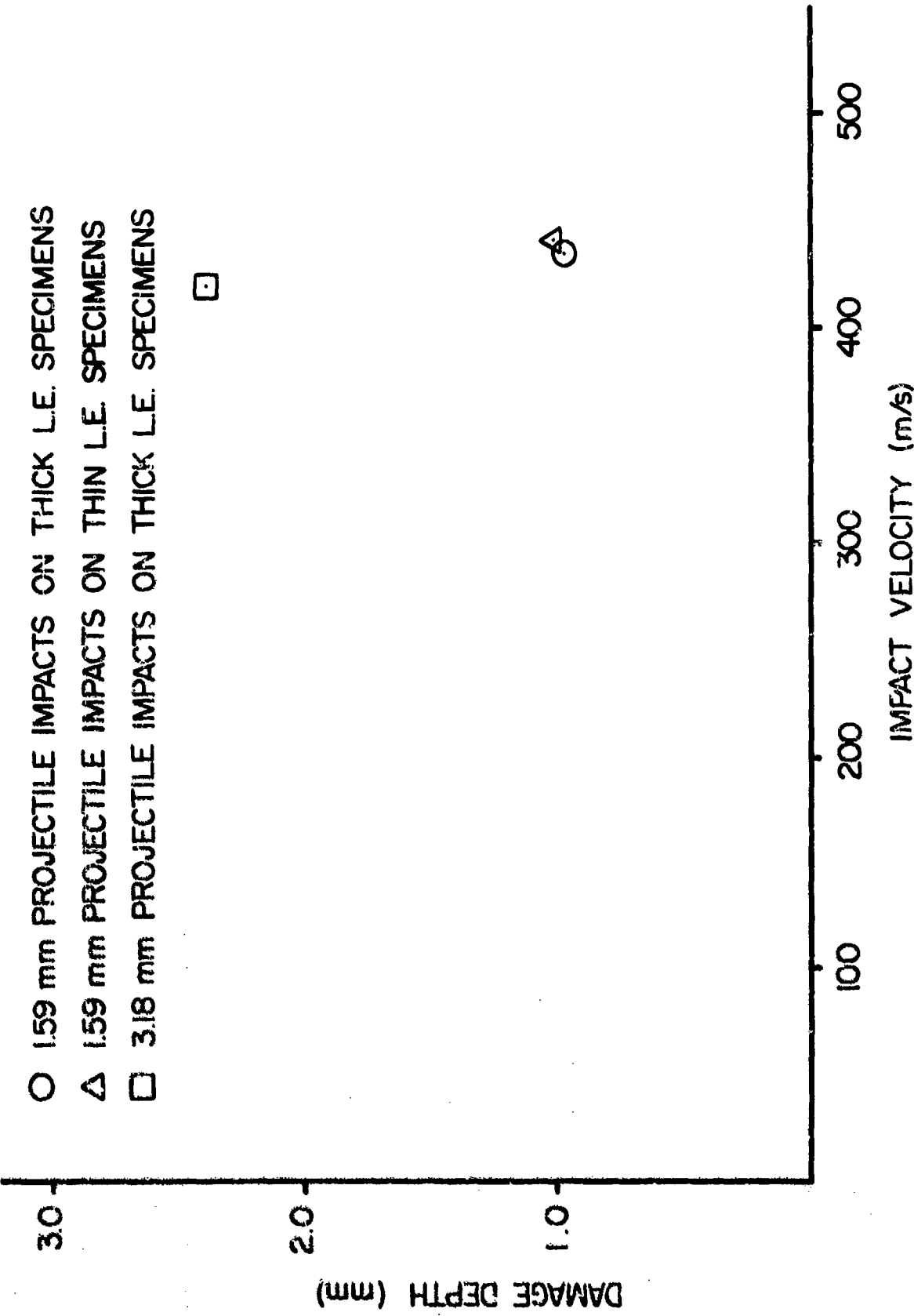
Figure 29. Plot of Damage Depth Versus Impact Velocity for Boron/Aluminum Specimens.

O   1.59 mm PROJECTILE IMPACTS ON THICK L.E. SPECIMENS

△   1.59 mm PROJECTILE IMPACTS ON THIN L.E. SPECIMENS

□   3.18 mm PROJECTILE IMPACTS ON THICK L.E. SPECIMENS

DAMAGE DEPTH (mm)

IMPACT VELOCITY (m/s)

54
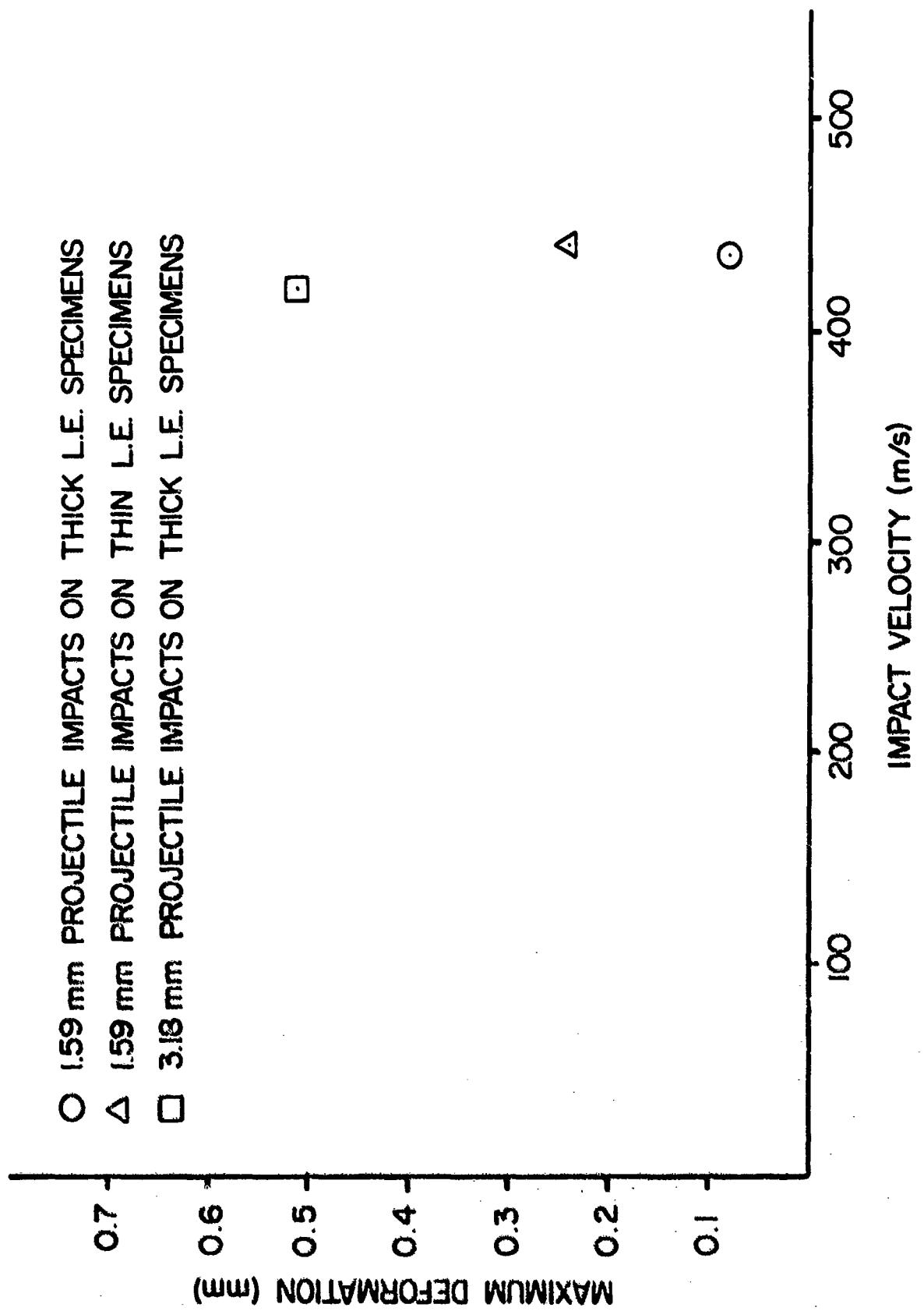
Figure 30. Plot of Maximum Plastic Deformation Damage Versus Impact Velocity for Boron/Aluminum Specimens.

○ 1.59 mm PROJECTILE IMPACTS ON THICK L.E. SPECIMENS
△ 1.59 mm PROJECTILE IMPACTS ON THIN L.E. SPECIMENS
□ 3.18 mm PROJECTILE IMPACTS ON THICK L.E. SPECIMENS

IMPACT VELOCITY (m/s)

MAXIMUM DEFORMATION (mm)

The damage received for the two leading edge thickness impacts was very similar in appearance. For the 18.9 degree impact at similar velocities, the 1.30 mm thick specimens had damage values of 2.18 mm for the width, 2.40 for the depth, and 0.51 mm for the plastic deformation. In the case for the 0.97 mm thick specimens the damage values was 0.97 mm for the width, 1.02 mm for the depth, and 0.19 mm for the plastic deformation. Based on these measurements, the damage on the thinner specimen was 11 percent too low for the width, 15 percent too low for the depth, and 25 percent too low for the plastic deformation for linear scaling to be applicable. In every case, the damage values were too low which can be attributed to the thickness of 0.97 mm for the half scale specimens being greater than required. Thus, attempting to compare the two thickness groups with the concept of geometric scaling cannot be made.

Typical damage received on the three impact groups are shown in Figures 31 through 33.

3.3   PEBBLE AND ICE BALL IMPACTS

A summary of the damage results for the various projectile and specimen types os presented in Table 8. Impacts at similar test conditions are grouped together and average. The number in parenthesis in the table indicates the number of tests (impactor type size, and velocity) in that group).

3.3.1   Results on Stainless Steel Specimens

A series of leading edge pebble impacts on 1.22 mm leading edge thick 403 stainless steel specimens was conducted at impact velocities of about 250 m/s. The impacts were conducted at two angles of incidence of 36.4 and 51.1 degrees. No visual damage was received on the specimens except for a pitted leading edge.

Typical damage on the specimens at the different impact angles are shown in Figures 34 and 35.

3.3.2   Results on Titanium Specimens

A series of leading edge impacts of pebbles and ice balls against 0.81 mm 8-1-1 titanium leading edges was conducted

Table 8. Summation of Pebble and Ice Sphere Impacts

Specimen Type	Specimen Leading Edge Thickness (mm)	Projectile Type and Size (mm)	Impact Velocity (m/s)	Impact Angle (°)	Remarks	Maximum Deformation Damage (mm)
403SS(5)	1.22	Pebble 6.35	242	35.4	Pitted Leading Edge	--
403SS(6)	1.22	Pebble 6.35	249	51.1	Pitted Leading Edge	--
8-1-1 Ti(5)	0.81	Pebble 6.35	406	24.4	Pitted Leading Edge With Deformation	0.23
8-1-1 Ti(5)	0.81	Pebble 6.35	298	41.0	Pitted Leading Edge With Deformation	0.45
8-1-1 Ti(3)	0.81	Ice Ball 25.40	365	24.4	Slight Deformation	0.23
8-1-1 Ti(2)	0.81	Ice Ball 25.40	221	41.0	Slight Deformation	1.18
APSI Blade(2)	1.59	Pebble 6.35	187	90.0	Partial Penetration With Bulge and Crack	--
APSI Blade(1)	1.59	Pebble 6.35	242	90.0	Complete Penetration With Bulge and Crack	--

Note: Number in parenthesis indicates number of tests conducted in that group.

57
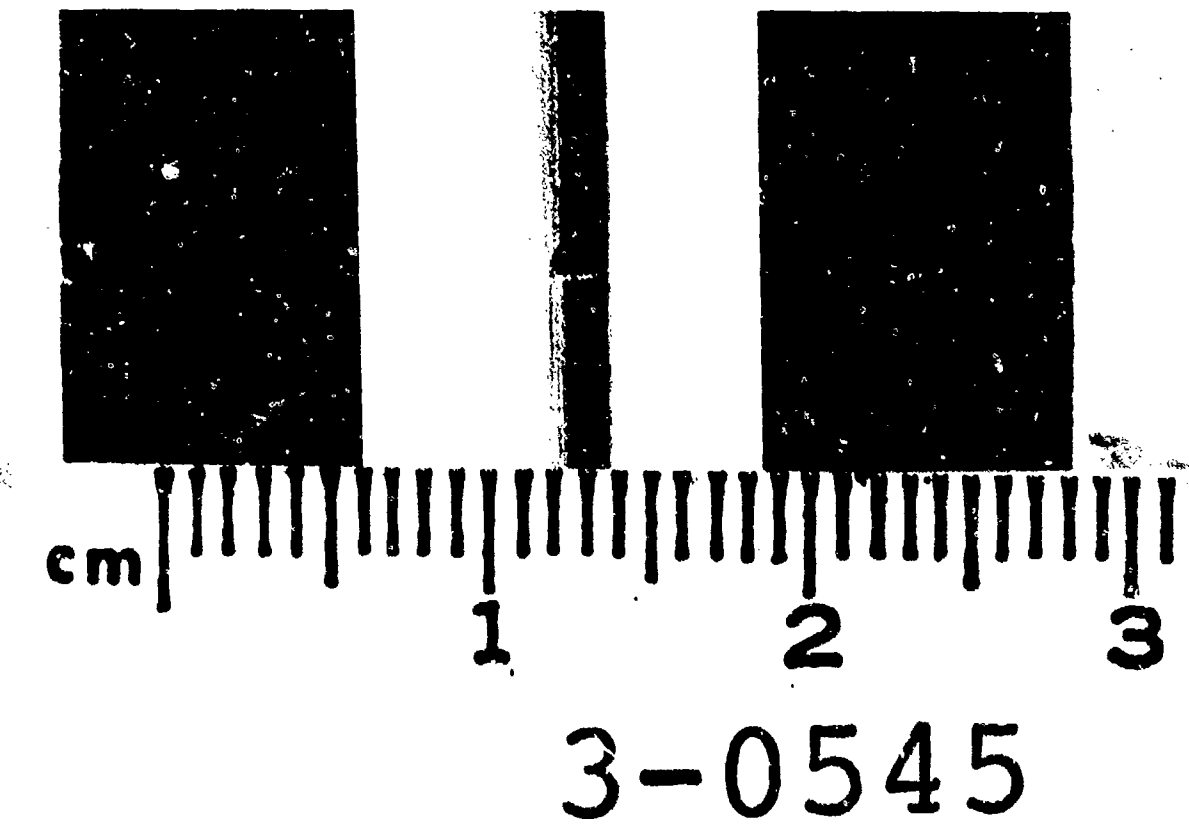
Figure 31.   Typical Damage Received on Thick Leading Edge
             Boron/Aluminum Specimens from 1.59 mm Projectile
             Impacts at 18.9°.

Figure 32. Typical Damage Received on Thick Leading Edge Boron/Aluminum Specimens from 3.18 mm Projectile Impacts at 18.9°.
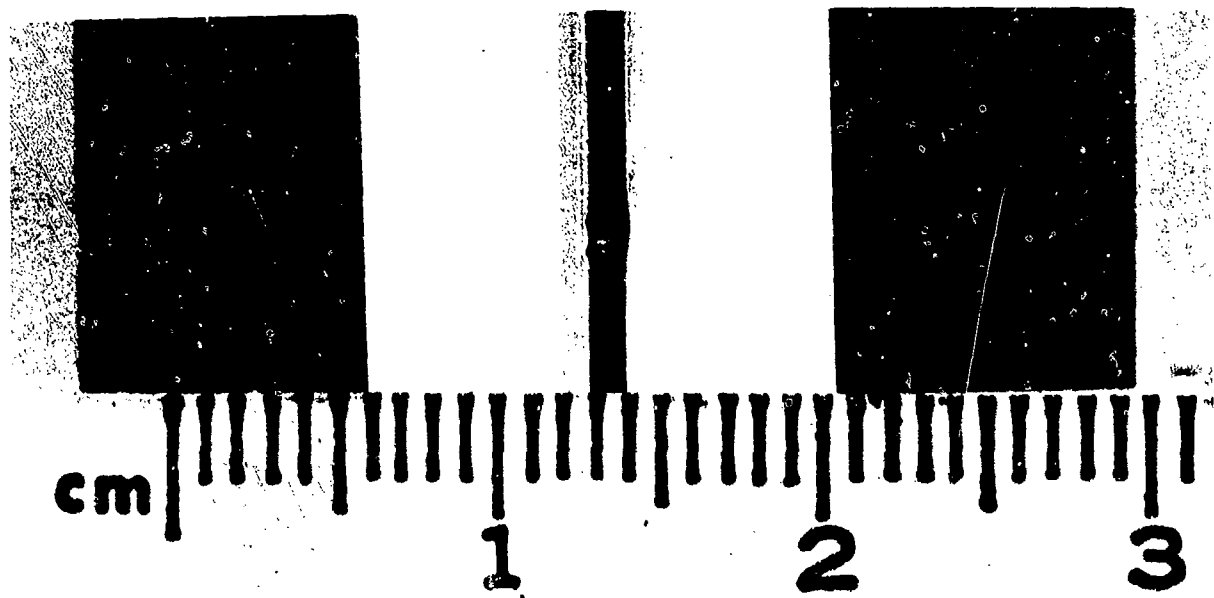
3-0553

Figure 33. Typical Damage Received on Thin Leading Edge
Boron/Aluminum Specimens from 1.59 mm Projectile
Impacts at 18.9°.
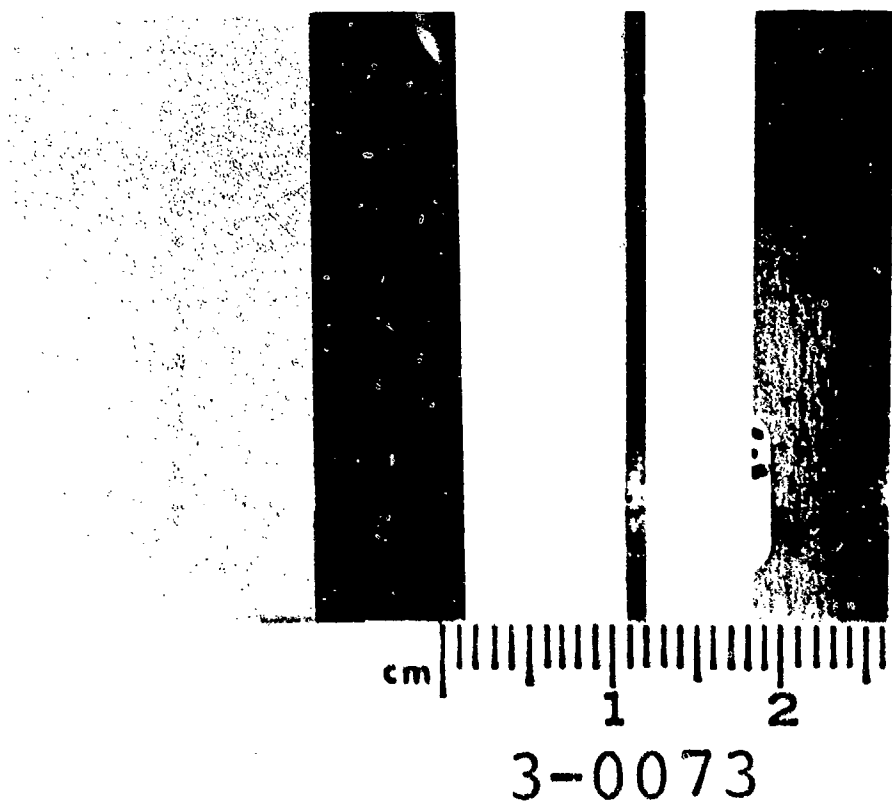
Figure 34.   Typical Damage Received on Stainless Steel
Specimens from Pebble Impacts at 36.4°.

3-0077
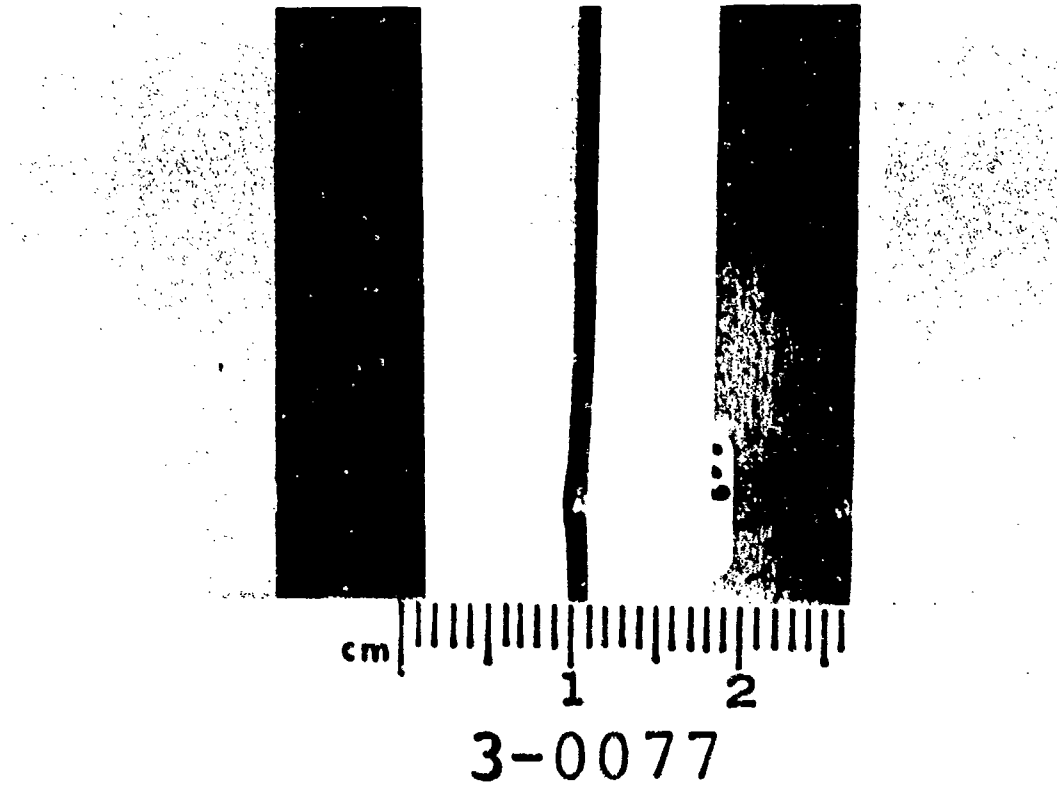
Figure 35.   Typical Damage Received on Stainless Steel
             Specimens from Pebble Impacts at 51.1°.

at angles of incidence of 24.4 and 41.0 degrees. The pebble impacts
at velocities of about 400 m/s at 24.4 degrees gave damage of a
pitted surface with a slight plastic deformation of 0.23 mm. The
pebble impacts at 300 m/s and 41.0 degrees generated damage of a
pitted surface with a larger plastic deformation of 0.45 mm.
Figure 36 shows typical damage received from pebble impact.

The 25.4 mm diameter ice ball impacts at a velocity
of 365 m/s and impact angle of 24.4 degrees resulted in generating
plastic deformation damage of 0.23 mm. Increasing the impact angle
to 41.0 degrees and decreasing the velocity to 220 m/s resulted in
increasing the plastic deformation to 1.18 mm. Figure 37 shows
typical damage received from an ice ball impact.

3.3.3 Results on APSI Blades

Three leading edge impacts of pebbles on APSI blades
were conducted at velocities of 187 and 242 m/s and an angle of
incidence of 90.0 degrees. In all cases, the projectile broke up
during the impact event. Two of the velocities at 187 m/s generated
damage of partial penetration with a bulge and crack at 242 m/s
resulted in complete penetration damage with a bulge and crack.

Figures 38 and 39 show the typical damage received
for the two velocities utilized.

3.4 ARTIFICIAL BIRD IMPACTS

A series of 85 gram artificial bird impacts was conducted
on the metal specimens. Table 9 presents a summary of the damage
results for the bird impacts on the various specimen types. A
number of preload (specimen loaded in tension to simulate centri-
fugal force effects of rotating fan system) tests was also con-
ducted on the stainless steel specimens. Impacts at similar test
conditions are grouped together in Table 9 and averaged. The
number in parenthesis in the table indicates the number of tests
in that group.

63

Table 9. Summation of 85 g. (3 ounce) Artificial Bird Impacts

Specimen Type	Specimen Leading Edge Thickness (mm)	Mounting Type	Pre-Stress Load (lbs)	Impact Velocity (m/s)	Impact Mass (g)	Impact Angle (°)	Remarks	Plastic Deformation Damage Leading Edge (mm)	Trailing Edge (mm)
403SS(1)	1.22	Free-Free	--	182	51.3	25.5	Plastic Deformation at Impact Site.	12.7	11.9
403SS(1)	1.22	Free-Free	--	193	53.6	36.4	Plastic Deformation at Impact Site.	65.5	52.3
403SS(1)	1.22	Free-Free	--	239	45.2	36.4	Plastic Deformation at Impact Site.	6.1	4.6
403SS(3)	1.22	Free-Free	--	246	66.1	36.4	Specimen Bent into Horseshoe Shape at Impact Site.	--	--
403SS(1)	1.22	Cantilever	--	235	76.4	36.4	Plastic Deformation at Impact Site. Specimen twisted 24.9mm from tip to tip.	141.7	114.3
403SS(2)	1.22	Free-Free	--	181	49.4	51.1	Plastic Deformation at Impact Site.	69.6	57.4
410SS(1)	0.61	Free-Free	--	245	47.5	36.4	Specimen Bent,Twisted and Mangled Severely. Severe Specimen	--	--
410SS(1)	0.61	Free-Free	--	168	--	51.1	Bending and Twist.	--	--
403SS(1)	1.22	Fixed-Fixed	3245	231	57.3	36.4	Plastic Deformation of Specimen at Impact Site.	18.3	3.6
403SS(1)	1.22	Fixed-Fixed	4019	181	56.4	51.1	Plastic Deformation of Specimen at Impact Site.	20.6	4.3
410SS(1)	3.61	Fixed-Fixed	1714	240	--	36.4	Specimen Bent and Twisted Severely.	--	--
410SS(1)	0.61	Fixed-Fixed	2025	--	--	51.1	Severe Plastic Deformation of Specimen.	--	--
8-1-1 Ti(1)	0.81	Free-Free	--	370	41.4	24.4	Plastic Deformation of Specimen.	4.1	--
8-1-1 Ti(1)	0.81	Free-Free	--	248	59.6	36.4	Plastic Deformation of Specimen.	20.0	--
8-1-1 Ti(1)	0.81	Free-Free	--	311	16.7	41.0	No Visual Damage.	--	--
3-1-1 Ti(1)	0.81	Free-Free	--	--	--	51.0	No Visual Damage.	--	--

Note: Number in Parenthesis indicates number of tests conducted in that group.
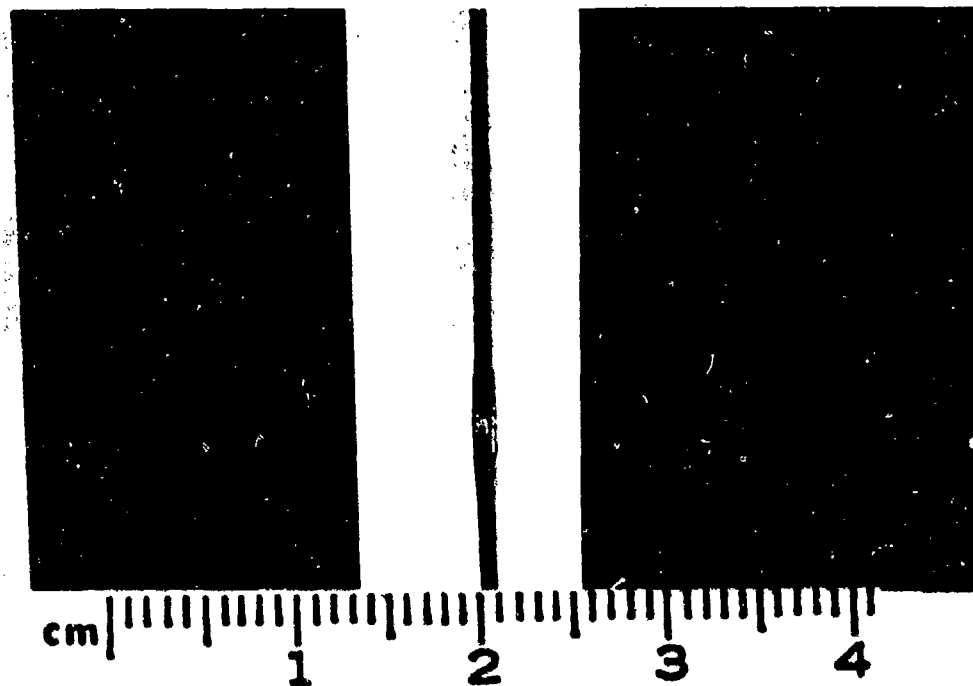
3-0245

Figure 36.   Typical Damage Received on Titanium Specimens from
Pebble Impacts at 41.0°.
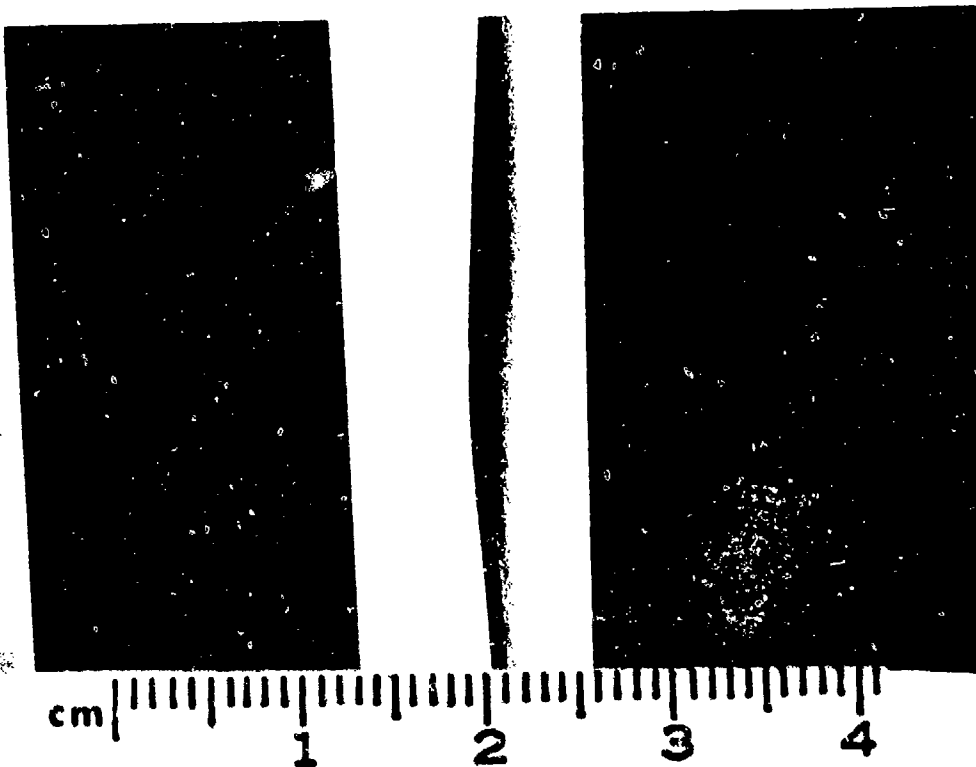
Figure 37.   Typical Damage Received on Titanium Specimens from
Ice Ball Impacts at 41.0°.
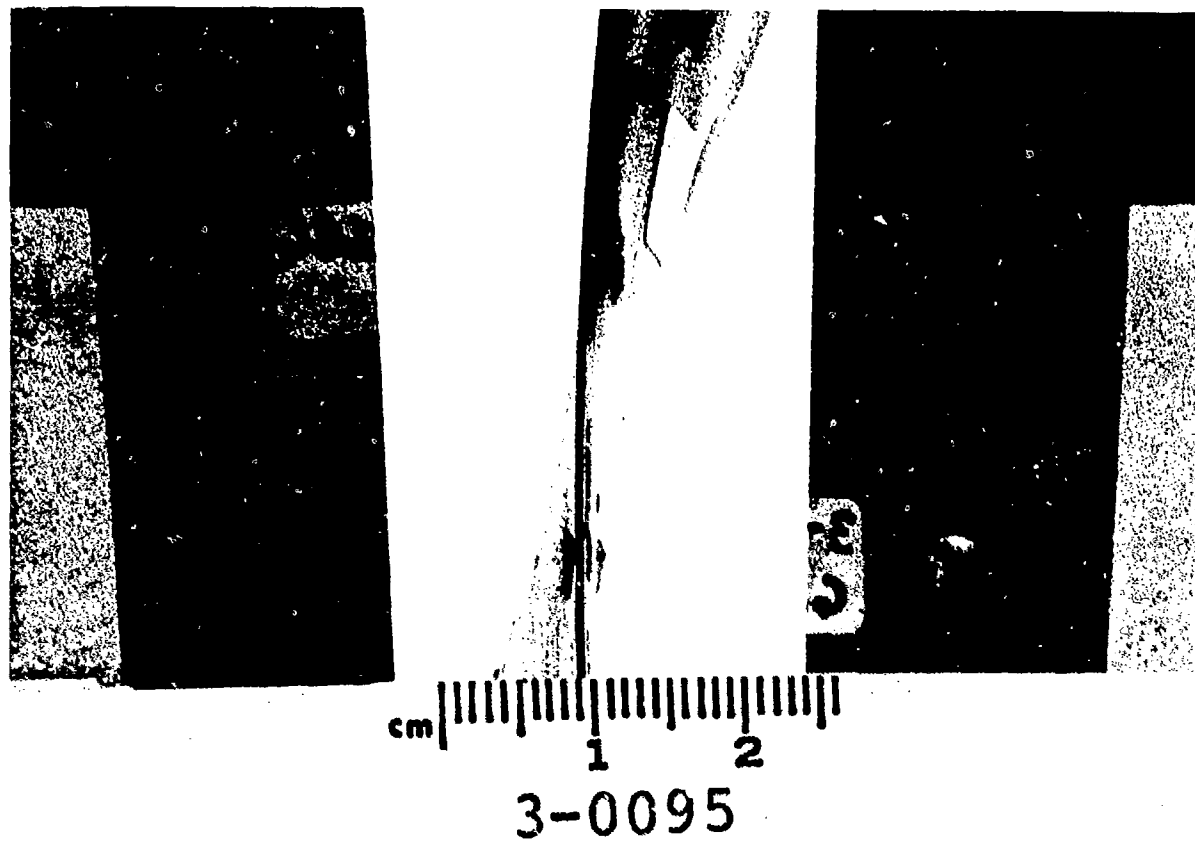
Figure 38.   Typical Damage Received on APSI Blade from
Pebble Impact at 187 m/s.
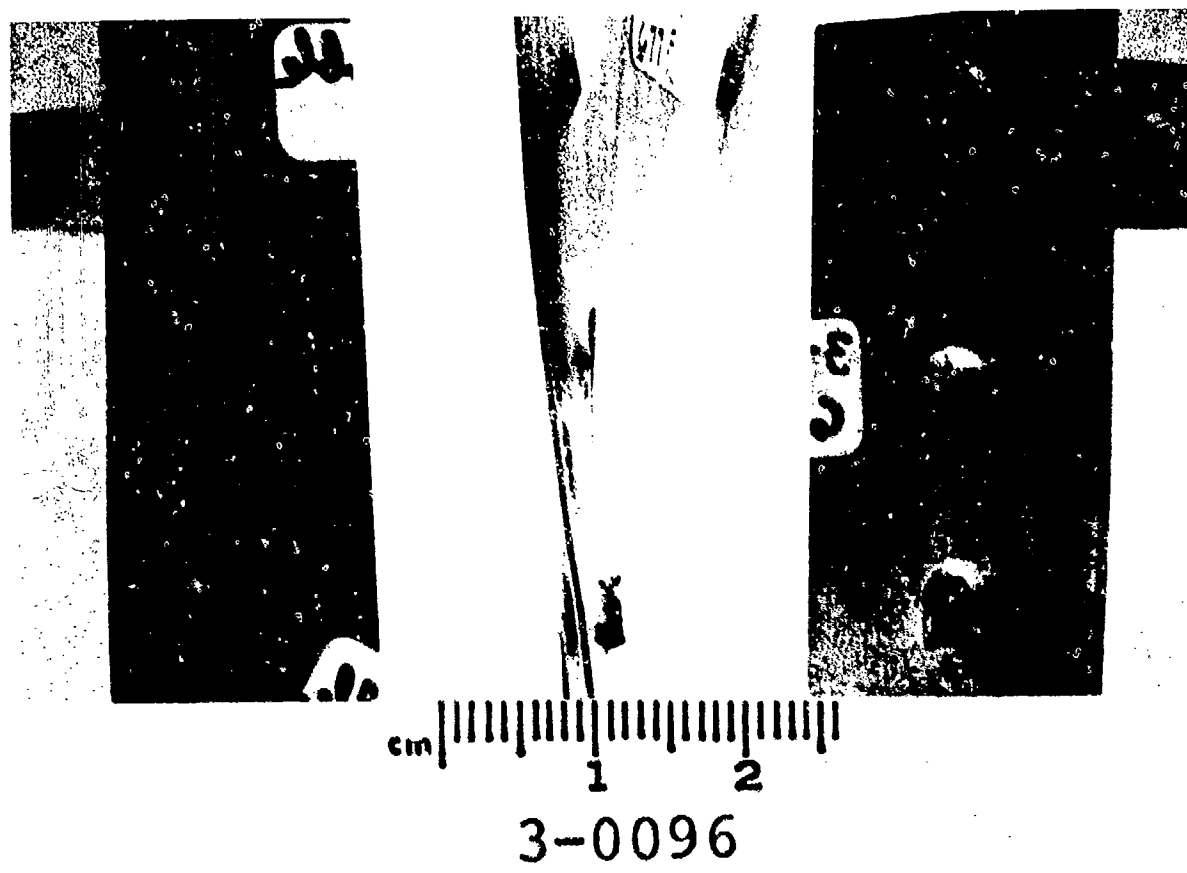
Figure 39. Typical Damage Received on APSI Blade from Pebble Impact at 242 m/s.

3.4.1   Results of Stainless Steel Specimens

A series of fifteen 85 gram artificial bird impacts was conducted on stainless steel specimens. The angles of incidence for the impacts were either 25.5, 36.4 or 51.1 degrees and the impact velocities ranged from 168 to 246 m/s. The mass of the bird which actually loaded the specimens ranged from 45.2 to 76.4 grams. In several cases, the impact mass of the artificial birds could not be determined because of the severe specimen damage received and the break-up of the bird during the impact event. Above a velocity of about 240 m/s and a bird impact mass of 45 gram , the nominal leading edge thickness of 1.22 mm for the 403 stainless steel specimens received severe bending damage at the impact site which resulted in several cases of bending the specimen into a horseshoe shape as shown in Figure 40. At test conditions below these levels, the damage was severe; however, the plastic deformation damage was measurable for the leading and trailing edges as shown in Figures 41 and 42. The half scale 410 stainless steel specimens received severe bending at the impact site which was unmeasurable for an impact velocity as low as 168 m/s as shown in Figure 43. In one case, a thicker leading edge specimen was cantilever mounted to determine if the resulting damage from an impact would be similar to that received for free-free mounted specimens. The damage was again severe in regards to bending at the impact site for the cantilevered specimen; however, a substantial twist was also received as shown in Figure 44.

The preload impact tests were conducted on both leading edge thickness specimens at angles of incidence of 36.4 and 51.1 degrees. The tensile stress for the 36.4 degree impacts was approximately 12 Ksi and 15 Ksi for the 51.1 degree impacts. For the nominal leading edge thickness specimens of 1.22 mm, the damage was plastic deformation at the impact site; however, it was measurable and substantially less severe than for the non-stressed specimen impacts. In the case of the preload tests on the 0.61 mm (half scale) leading edge specimens, the plastic deformation was very severe and unmeasurable. Figures 45 and 46

2-0072
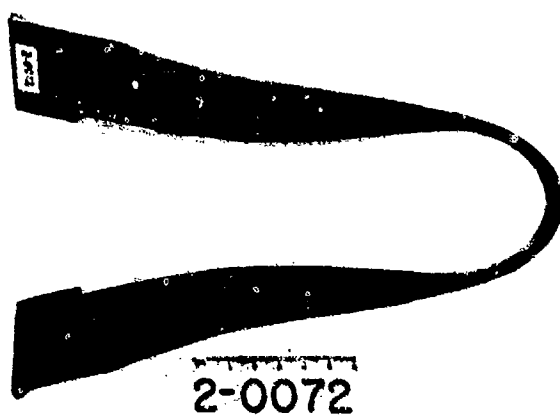
Figure 40. Typical Severe Bending Damage for 85 gram Bird
Impact on 403 Stainless Steel Specimens.

2-0069

Figure 41. Typical Measurable Damage on 403 Stainless Steel
Specimens from 85 gram Bird Impact at 36.4°.

2-0074

Figure 42. Typical Measurable Damage on 403 Stainless Steel
            Specimens from 85 gram Bird Impact at 51.1°.

2-0079
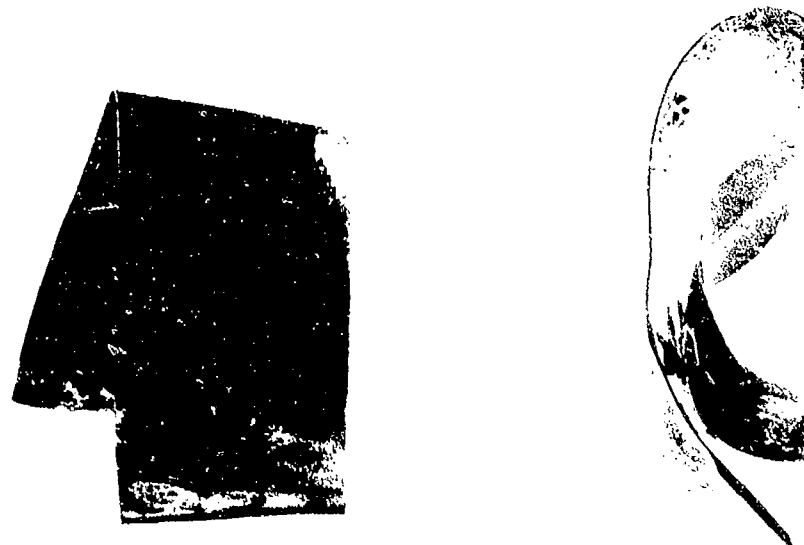
Figure 43. Typical Severe Bending Damage for 85 gram Bird
            Impact on Half-Scale 410 Stainless Steel Specimens.

2-0075
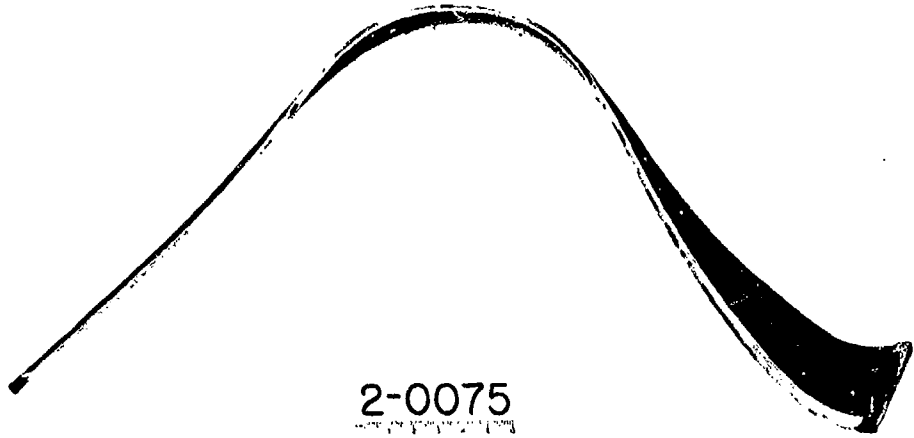
Figure 44.   Bending and Twist Damage on Cantilever Mounted
             403 Stainless Steel Specimen from 85 gram Bird
             Impact at 36.4°.

2-0082

Figure 45.   Damage on 1.22 mm Thick Leading Edge Specimen in
             Preload Test.

2-0084

Figure 46.   Damage on 0.61 mm Thick Leading Edge Specimen
             in Preload Test.

73

show the resulting damage for the 1.22 mm and 0.61 mm thick leading edge specimens, respectively.

Due to the severe damage received for the small (85 gram) bird impacts, the large bird (680 gram) impacts were deleted from the testing. The impact mass of the large bird would have been about four times greater than for the small bird. Since the specimens were flat without camber or twist, the stiffness of the test specimens is much lower than for the actual blades. It was felt that the large bird impacts would result in overpowering the flat specimens and the data would be meaningless.

The damage for the small bird impacts was in the form of severe plastic deformation or bending without any visible cracking. Thus, the residual strength of the specimens would not be affected.

3.4.2 Results of Titanium Specimens

A series of four impacts of 85 gram birds was conducted of 0.81 mm thick leading edge 8-1-1 Ti specimens. All of the impacts were conducted at different angles of incidence. At angles of incidence of 24.4 and 36.4 degrees and velocities of 370 and 248 m/s, respectively, the damage was in the form of moderate plastic deformation of the specimen leading edge. No visible damage was received for the 41.0 and 51.1 degree impacts at velocities of about 300 m/s.

Photographs of damaged and non-damaged specimens are shown in Figures 47 and 48, respectively.

74

2-0086

Figure 47.   Photograph Showing Damage on Titanium Specimen
from 85 gram Bird Impact.

2-0087

Figure 48.   Photograph Showing No Damage on Titanium Specimen
from 85 gram Bird Impact.

SECTION IV
SUMMARY AND CONCLUSIONS

Leading edge impact damage was studied by performing a series
of hard particle and soft body impact tests on small test specimens
fabricated of typical blade materials. The three fan blade type
materials investigated were the J79 blade material of 403 stainless
steel, the F101 blade material of 8Al-1Mo-IV (8-1-1) titanium, and
the APSI metal matrix blade material of boron/aluminum. The local
damage problem was investigated on the three materials using glass
beads, steel spheres, granite pebbles, ice, and artificial bird as
the impactors. A number of general conclusions drawn from the data
generated in this study is given in the following paragraphs.

4.1   GLASS BEAD IMPACTS

Slight damage resulted from the leading edge impacts with
the glass beads breaking up upon impact. Chrome steel spheres were
substituted for the glass beads to avoid the uncertainty surrounding
the effect of projectile break up upon the damage inflicted on the
targets.

4.2   CHROME STEEL SPHERE IMPACTS

Preliminary testing indicated that minimal damage was received
from 0.76 mm (30 mil) steel sphere impacts. The size of the spheres
was increased to 1.39 and 3.18 mm diameter to receive measureable
damage from the leading edge impacts.

4.2.1   Stainless Steel Material

The resulting damage from the steel sphere impacts
was in the form of a dent or dimple with a bulge. No cracks or
tearing were observed at the impact site which indicated the impact
velocities were below critical values where a bulge with a tear
results. The concept of geometric scaling was investigated by per-
forming a series of tests using different leading edge thicknesses
and different projectile sizes. The damage for the two thicknesses

was very similar in appearance; however, the concept of geometry scaling did not seem to work as well as expected. The scaling seemed to be fairly good for the width and depth damage and fair for the maximum deformation damage.

4.2.2   Titanium Material

The damage generated in titanium from steel sphere impacts was in the form of mass loss from the specimen leading edge which indicated that the impact velocities were above the critical velocity value where a bulge with a rip or tear occurs. The damage was greater in value for the 41.0 degree impacts at a lower velocity than for the 24.4 degree impacts. In all cases, the impacts generated negigible plastic deformation on the specimens.

4.2.3   Boron/Aluminum Material

The type of damage received for two different thickness specimens from two different size projectile impacts was in the form of nicks with very little bulging. In several cases, the outer skin of the nickel leading edge protection material was rolled back; however, there were no rips or tears generated which indicated the impact velocity was below the critical value.

The concept of geometric scaling was investigated; however, it did not work as well as expected. One reason that contributed to the scaling not working was that the overall thickness of the leading edge of the nominal and half-scale specimens were very much alike. Based on the damage measurements; the damage for the 0.97 mm thick specimens was low by as much as 25 percent for linear scaling to be applicable. However, the damage received for the two thickness specimens was very similar in appearance.

4.3   PEBBLE AND ICE BALL IMPACTS

A number of impact tests using pebble and ice ball projectiles was conducted on the three materials investigated.

77

4.3.1   Stainless Steel

No visual damage was received for pebble impacts on the stainless steel specimens except for a pitted leading edge at the impact site.

4.3.2   Boron/Aluminum APSI Blades

Two leading edge impacts from pebbles generated damage of partial penetrations with a bulge and crack at the impact sites for impact velocities of 187 m/s and an impact angle of 90 degrees. A 90.0 degree impact at a velocity of 242 m/s generated complete penetration with a bulge and crack.

4.3.3   Titanium Material

A series of leading edge impact tests was performed using pebble and ice ball impactors. The pebble impacts generated damage of a pitted surface at the impact site with a slight deformation. The ice ball impacts generated slight plastic deformation damage at the impact site.

4.4   ARTIFICIAL BIRD IMPACTS

A series of 85 gram artificial bird impacts were performed on the metal materials.

4.4.1   Stainless Steel

The small bird impacts on stainless steel generated severe bending damage at the impact site. Above a velocity of 240 m/s and a bird impact slice mass of 45 grams, the nominal leading edge thick specimens (1.22 mm thick) received severe bending at the impact site to plastically deform the specimens into a horseshoe shape. At test conditions below these levels, the damage was severe; however, the plastic deformation was measurable. The thinner specimens (0.61 mm thick) received severe bending which was unmeasurable for the small bird impacts at velocities as low as 170 m/s.

A series of preload impact tests were also performed on the stainless steel material to determine its response to impact.

Tensile stresses of about 12 and 15 Ksi were used to simulate the effect of centrifugal force of a rotating fan system. The damage for the thicker specimens was in the form of plastic deformation; however, it was measurable and substantially less severe than for the nonstressed specimen impacts. The damage for the thinner specimens in the preload tests was in the form of severe plastic deformation which was unmeasurable.

In all cases, the damage was severe; however, there were no visible cracks or tearing of the material which would affect the residual strength of the material.

4.4.2   Titanium Material

The small bird impacts on titanium specimens generated moderate plastic deformation at the impact site for angles of incidence of 24.4 and 36.4 degrees and impact velocities of 370 and 248 m/s, respectively.

Impacts at a velocity of about 300 m/s at impact angles of either 41.0 or 51.1 degrees produced no visible damage on the titanium material.

REFERENCES

1. Barber, John P., Taylor, H.R., and Wilbeck, James S.,
    "Characterization of Bird Impacts on a Rigid Plate:
    Part I", AFFDL-TR-75-5, January 1975.

2. Peterson, R. L., and Barber, John P., "Bird Impact Forces
    in Aircraft Windshield Design", AFFDL-TR-75-150, March 1976.

3. Barber, J. P., Wilbeck, J. S. and Taylor, H. R., "Bird
    Impact Forces and Pressures on Rigid and Compliant Targets",
    UDRI-TR-77-17.

4. Wilbeck, J. S., "Soft Body Impact", Ph.D. Dissertation,
    Texas A&M University, in-preparation, May 1977.

5. Nicholas, T., Barber, J. P., and Bertke, R. S., "Impact
    Damage on Titanium Leading Edges From Small Hard Objects",
    AFML-TR-78-173, November 1978.

Shot#	Material	Size (cm)	Leading Edge Thickness (mm)	Impact Angle (°)	Support Method	Projectile Type Size (mm)	Velocity (m/s)	Remarks
3-0019	403SS	15.2x5.66x0.46	1.22	51.1	Free Free	Pyrex Sphere 3.18	483	Projectile Broke on Impact.
3-0020	403SS	15.2x5.66x0.46	1.22	51.1	Free Free	Pyrex Sphere 3.18	434	Projectile Broke on Impact.
3-0036	F-101 Blade			51.1	Free Free	Pyrex Sphere 3.18	520	Projectile Broke on Impact.
3-0039	APSI Blade			38.8	Free Free	Pyrex Sphere 1.59	est 427	Projectile Broke on Impact.
3-0041	APSI Blade			38.8	Free Free	Glass Shot 0.79	est 427	Projectile Broke on Impact.
1-0042	APSI Blade			38.8	Free Free	Pyrex Sphere 3.18	292	Projectile Broke on Impact.
3-0043	APSI Blade			38.8	Free Free	Pyrex Sphere 3.18	428	Projectile Broke on Impact.

81

Shot#	Material	Size (cm)	Impact Angle (°)	Support Method	Projectile Size (mm)	Velocity (m/s)	Remarks	Max Deformation (mm)	Damage Width (mm)	Damage Depth (mm)
3-0044	403SS	15.2x5.66x0.46	51.1	Free Free	Chrome Steel Sphere 1.59	174	Dimple on Edge	0.000	1.28	0.18
3-0045	403SS	15.2x5.66x0.46	51.1	Free Free	Chrome Steel Sphere 1.59	150	Dimple on Edge	0.000	1.10	0.15
3-0046	403SS	15.2x5.66x0.46	51.1	Free Free	Chrome Steel Sphere 1.59	est 171	Dimple on Edge	0.000	1.28	0.18
3-0047	403SS	15.2x5.66x0.46	51.1	Free Free	Chrome Steel Sphere 1.59	176	Dimple on Edge	0.000	1.31	0.20
3-0048	403SS	15.2x5.66x0.46	51.1	Free Free	Chrome Steel Sphere 1.59	est 171	Dimple on Edge	0.000	1.21	1.77
3-0050	403SS	15.2x5.66x0.46	51.1	Free Free	Chrome Steel Sphere 3.18	154	Dent and Bulge	0.203	2.53	0.41
3-0051	403SS	15.2x5.66x0.46	51.1	Free Free	Chrome Steel Sphere 3.18	180	Dent and Bulge	0.305	2.73	0.52
3-0052	403SS	15.2x5.66x0.46	51.1	Free Free	Chrome Steel Sphere 3.18	183	Dent and Bulge	0.457	2.51	0.46
3-0053	403SS	15.2x5.66x0.46	51.1	Free Free	Chrome Steel Sphere 3.18	180	Dent and Bulge	0.381	2.71	0.53
3-0054	403SS	15.2x5.66x0.46	51.1	Free Free	Chrome Steel Sphere 3.18	175	Dent and Bulge	0.432	2.31	0.39
3-0055	403SS	15.2x5.66x0.46	51.1	Free Free	Chrome Steel Sphere 3.18	181	Dent and Bulge	0.432	2.65	0.50

Shot	Material	Size (cm)	Impact Angle (°)	Support Method	Projectile Size (mm)	Velocity (m/s)	Remarks	Max. Deformation (mm)	Damage Width (mm)	Depth (mm)
3-0056	4035S	15.2x5.66x0.46	36.4	Free Free	Chrome Steel Sphere 1.59	225	Dimple on Edge	0.051	1.26	0.14
3-0057	4035S	15.2x5.66x0.46	36.4	Free Free	Chrome Steel Sphere 1.59	131	Dimple on Edge	--	0.98	0.07
3-0058	4035S	15.2x5.66x0.46	36.4	Free Free	Chrome Steel Sphere 1.59	254	Dimple and Bulge	0.178	1.03	0.06
3-0060	4035S	15.2x5.66x0.46	36.4	Free Free	Chrome Steel Sphere 1.59	est 263	Dimple on Edge	--	1.06	0.09
3-0061	4035S	15.2x5.66x0.46	36.4	Free Free	Chrome Steel Sphere 1.59	262	Dimple on Edge	--	1.38	0.25
3-0062	4035S	15.2x5.66x0.46	36.4	Free Free	Chrome Steel Sphere 1.59	163	Dimple on Edge	0.203		
3-0063	4035S	15.2x5.66x0.46	36.4	Free Free	Chrome Steel Sphere 1.59	240	Dimple and Bulge	0.254	1.13	0.07
3-0064	4035S	15.2x5.66x0.46	36.4	Free Free	Chrome Steel Sphere 1.59	234	Dimple and Bulge	0.254	1.12	0.05
3-0065	4035S	15.2x5.66x0.46	36.4	Free Free	Chrome Steel Sphere 3.18	236	Dent and Bulge, Also Cracked	0.635	2.97	0.69
3-0066	4035S	15.2x5.66x0.46	36.4	Free Free	Chrome Steel Sphere 3.18	240	Dent and Bulge	0.559	2.85	0.72
3-0067	4035S	15.2x5.66x0.46	36.4	Free Free	Chrome Steel Sphere 3.18	239	Dent and Bulge	0.584	2.66	0.70
3-0068	4035S	15.2x5.66x0.46	36.4	Free Free	Chrome Steel Sphere 3.18	245	Dent and Bulge	--	2.41	0.49
3-0069	4035S	15.2x5.66x0.46	36.4	Free Free	Chrome Steel Sphere 3.18	240	Dent and Bulge	0.762	2.96	0.72

Shot#	Material	Size (cm)	Impact Angle (°)	Support Method	Projectile Size (mm)	Velocity (m/s)	Remarks	Max Deformation (mm)	Damage Width (mm)	Damage Depth (mm)
3-0110	410SS	15.2x5.66x0.23	51.1	Free Free	Chrome Steel Sphere 1.59	170	Dimple and Bulge	0.330	1.19	0.39
3-0111	410SS	15.2x5.66x0.23	51.1	Free Free	Chrome Steel Sphere 1.59	182	Dimple and Bulge	0.203	1.23	0.23
3-0112	410SS	15.2x5.66x0.23	51.1	Free Free	Chrome Steel Sphere 1.59	163	Dimple and Bulge	0.203	1.19	0.19
3-0113	410SS	15.2x5.66x0.23	51.1	Free Free	Chrome Steel Sphere 1.59	182	Dimple and Bulge	0.279	1.28	0.22
3-0114	410SS	15.2x5.66x0.23	51.1	Free Free	Chrome Steel Sphere 1.59	174	Dimple and Bulge	0.305	1.21	0.20
3-0115	410SS	15.2x5.66x0.23	36.4	Free Free	Chrome Steel Sphere 1.59	242	Dimple and Bulge	0.406	1.40	0.36
3-0116	410SS	15.2x5.66x0.23	36.4	Free Free	Chrome Steel Sphere 1.59	241	Dimple and Bulge	0.457	1.42	0.26
3-0117	410SS	15.2x5.66x0.23	36.4	Free Free	Chrome Steel Sphere 1.59	244	Dimple and Bulge	0.381	1.29	0.36
3-0118	410SS	15.2x5.66x0.23	36.4	Free Free	Chrome Steel Sphere 1.59	243	Dimple and Bulge	0.432	1.26	0.27
3-0119	410SS	15.2x5.66x0.23	36.4	Free Free	Chrome Steel Sphere 1.59	est 242	Dimple and Bulge	0.559	1.48	0.31

84

Shot#	Material	Size (cm)	Impact Angle (°)	Support Method	Projectile Size (mm)	Velocity (m/s)	Remarks	Damage Width (mm)	Depth (mm)
3-0218	8-1-1 Ti	15.2x8.86x0.43	41.0	Free Free	Chrome Steel Sphere 3.18	306	Dent & Crack Impact Below Edge.	--	--
3-0219	8-1-1 Ti	15.2x8.86x0.43	41.0	Free Free	Chrome Steel Sphere 3.18	306	Dent.	1.84	0.25
3-0220	8-1-1 Ti	15.2x8.86x0.43	41.0	Free Free	Chrome Steel Sphere 3.18	305	Mass Loss on Leading Edge.	3.17	1.55
3-0221	8-1-1 Ti	15.2x8.86x0.43	41.0	Free Free	Chrome Steel Sphere 3.18	314	Dimple & Bulge.	15.06	1.14
3-0222	8-1-1 Ti	15.2x8.86x0.43	41.0	Free Free	Chrome Steel Sphere 3.18	310	Mass Loss on Leading Edge.	3.17	1.66
3-0223	9-1-1 Ti	15.2x8.86x0.43	41.0	Free Free	Chrome Steel Sphere 3.18	314	Mass Loss on Leading Edge.	3.09	1.05
3-0224	8-1-1 Ti	15.2x8.86x0.43	41.0	Free Free	Chrome Steel Sphere 3.18	310	Mass Loss on Leading Edge.	3.26	1.40
3-0225	8-1-1 Ti	15.2x8.86x0.43	41.0	Free Free	Chrome Steel Sphere 1.59	311	Mass Loss on Leading Edge.	1.39	0.28
3-0226	8-1-1 Ti	15.2x8.86x0.43	41.0	Free Free	Chrome Steel Sphere 1.59	309	Mass Loss on Leading Edge.	2.50	0.42
3-0227	8-1-1 Ti	15.2x8.86x0.43	41.0	Free Free	Chrome Steel Sphere 1.59	304	Mass Loss on Leading Edge.	1.37	0.51
3-0228	8-1-1 Ti	15.2x8.86x0.43	41.0	Free Free	Chrome Steel Sphere 1.59	306	Mass Loss on Leading Edge.	1.41	0.48
3-0229	8-1-1 Ti	15.2x8.86x0.43	41.0	Free Free	Chrome Steel Sphere 1.59	308	Mass Loss on Leading Edge.	3.13	0.57

Shot#	Material	Size (cm)	Impact Angle (°)	Support Method	Projectile Size (mm)	Velocity (m/s)	Remarks	Damage Width (mm)	Damage Depth (mm)
3-0230	8-1-1 Ti	15.2x8.86x0.43	24.4	Free Free	Chrome Steel Sphere 1.59	350	Mass Loss on Leading Edge	1.36	0.61
3-0231	8-1-1 Ti	15.2x8.86x0.43	24.4	Free Free	Chrome Steel Sphere 1.59	381	Mass Loss on Leading Edge	1.55	0.61
3-0232	8-1-1 Ti	15.2x8.86x0.43	24.4	Free Free	Chrome Steel Sphere 1.59	385	Mass Loss on Leading Edge	1.57	0.53
3-0233	8-1-1 Ti	15.2x8.86x0.43	24.4	Free Free	Chrome Steel Sphere 1.59	391	Mass Loss on Leading Edge	1.44	0.66
3-0234	8-1-1 Ti	15.2x8.86x0.43	24.4	Free Free	Chrome Steel Sphere 1.59	428	Mass Loss on Leading Edge	1.19	0.25
3-0235	8-1-1 Ti	15.2x8.86x0.43	24.4	Free Free	Chrome Steel Sphere 1.59	378	Mass Loss on Leading Edge	1.59	0.57
3-0236	8-1-1 Ti	15.2x8.86x0.43	24.4	Free Free	Chrome Steel Sphere 3.18	377	Mass Loss on Leading Edge	3.10	2.21
3-0237	8-1-1 Ti	15.2x8.86x0.43	24.4	Free Free	Chrome Steel Sphere 3.18	386	Mass Loss on Leading Edge	3.07	1.39
3-0238	8-1-1 Ti	15.2x8.86x0.43	24.4	Free Free	Chrome Steel Sphere 3.18	410	Mass Loss on Leading Edge	3.22	1.61
3-0239	8-1-1 Ti	15.2x8.86x0.43	24.4	Free Free	Chrome Steel Sphere 3.18	389	Mass Loss on Leading Edge	3.37	2.14
3-0240	8-1-1 Ti	15.2x8.86x0.43	24.4	Free Free	Chrome Steel Sphere 3.18	403	Mass Loss on Leading Edge	3.13	1.41

Shot #	APSI Blade Like Specimen	Specimen No.	N. Plate Thickness (mm)	L.E. THK (mm)	T.E. THK (mm)	Impact Angle (°)	Support Method	Projectile Type Size (mm)	Velocity (m/s)	Remarks	Max Deforma- tion (mm)	Damage Width (mm)	Damage Depth (mm)
3-0540	Data Base	IV B1-2B	0.635	1.143	0.914	18.9	Free Free	Chrome Steel 0.79	427	Edge on Impacts Nicked the Edge	0.000	0.61	0.33
3-0541	Data Base	IV B1-1A	0.508	1.143	0.813	18.9	Free Free	Chrome Steel 1.59	471	Nicked the Edge	0.051	1.14	0.99
3-0542	Data Base	IV B1-4A	0.686	1.219	1.016	18.9	Free Free	Chrome Steel 1.59	445	Nicked the Edge	--	1.45	--
3-0543	Data Base	IV B1-4B	0.531	1.219	0.762	18.9	Free Free	Chrome Steel 1.59	440	Nicked the Edge, Also Slight Bulge	--	1.47	--
3-0544	Data Base	IV B1-5A	0.610	1.397	1.016	18.9	Free Free	Chrome Steel 1.59	367	Nicked the Edge	0.102	1.24	0.81
3-0545	Data Base	IV B1-5B	0.584	1.219	0.889	18.9	Free Free	Chrome Steel 1.59	449	Nicked the Edge	0.178	1.22	1.14
3-0546	Data Base	IV B1-10A	0.660	1.372	0.965	18.9	Free Free	Chrome Steel 3.18	381	Rolled Back Outer Skin	0.711	2.79	4.01
3-0547	Data Base	IV B1-15A	0.660	1.372	0.940	18.9	Free Free	Chrome Steel 3.18	450	Nicked the Edge	0.279	1.66	2.11
3-0548	Data Base	IV B1-15B	0.584	1.245	1.041	18.9	Free Free	Chrome Steel 3.18	403	Nicked the Edge, Rolled back Outer Edge	1.067	2.51	2.84
3-0549	Data Base	IV B1-16A	0.660	1.295	1.016	18.9	Free Free	Chrome Steel 3.18	409	Nicked the Edge, Rolled back Outer Edge	0.610	2.08	2.97
3-0550	Data Base	IV B1-16B	0.660	1.194	0.914	16.9	Free Free	Chrome Steel 3.18	447	Nicked the Back Rolled Back Outer Edge	0.432	1.85	2.06

Shot #	Rotor Blade Like Specimen	Specimen No.	H. Plate Thickness (mm)	L.E. THK (mm)	T.E. THK (mm)	Impact Angle (°)	Support Method	Projectile Type Size (mm)	Velocity (m/s)	Remarks	Max Deforma-tion(mm)	Damage Depth (mm)	Width (mm)
1-0551	Scale Effect	IV B1-128	0.279	1.016	0.686	18.9	Free Free	Chrome Steel 1.59	373	Nicked the Edge	0.229	0.86	1.14
1-0552	Scale Effect	IV B1-130	0.356	0.940	0.686	18.9	Free Free	Chrome Steel 1.59	400	Nicked the Edge	0.254	0.81	0.99
1-0552	Scale Effect	IV B1-131	0.305	1.041	0.737	18.9	Free Free	Chrome Steel 1.59	508	Nicked the Edge	0.254	1.32	1.07
1-0553	Scale Effect	IV B1-140	0.330	0.839	0.686	18.9	Free Free	Chrome Steel 1.59	462	Nicked the Edge	0.102	0.66	0.81
1-0555	Scale Effect	IV B1-145	0.330	0.940	0.787	18.9	Free Free	Chrome Steel 1.59	453	Nicked the Edge	0.127	1.22	1.07

Shot #	Material	Size (cm)	Impact Angle (°)	Support Method	Projectile Type Size (mm)	Velocity (m/s)	Remarks
3-0070	403SS	15.2x5.66x0.46	36.4	Free Free	STD. Pebble 6.35	234	Projectile Broke up on Impact Pitted the Edge of Specimen
3-0071	403SS	15.2x5.66x0.46	36.4	Free Free	STD. Pebble 6.35	245	Pitted the Edge
3-0072	403SS	15.2x5.66x0.46	36.4	Free Free	STD. Pebble 6.35	244	Pitted the Edge
3-0073	403SS	15.2x5.66x0.46	36.4	Free Free	STD. Pebble 6.35	239	Pitted the Edge
3-0074	403SS	15.2x5.66x0.46	36.4	Free Free	STD. Pebble 6.35	247	Pitted the Edge
3-0075	403SS	15.2x5.66x0.46	51.1	Free Free	STD. Pebble 6.35	246	Poor Shot - Missed Target
3-0076	403SS	15.2x5.66x0.46	51.1	Free Free	STD. Pebble 6.35	256	Pitted the Edge
3-0077	403SS	15.2x5.66x0.46	51.1	Free Free	STD. Pebble 6.35	250	Pitted the Edge
3-0078	403SS	15.2x5.66x0.46	51.1	Free Free	STD. Pebble 6.35	248	Pitted the Edge
3-0079	403SS	15.2x5.66x0.46	51.1	Free Free	STD. Pebblo 6.35	246	Pitted the Edge
3-0080	403SS	15.2x5.66x0.46	51.1	Free Free	STD. Pebble 6.35	250	Pitted the Edge

89

Shot#	Material	Size (cm)	Impact Angle (°)	Support Method	Projectile Type Size (mm)	Velocity (m/s)	Remarks	Max. Deformation Damage (mm)
3-0241	8-1-1 Ti	15.2x8.86x0.43	24.4	Free Free	STD. Pebble 6.35	445	Slight Deformation and Pitted Surface	0.13
3-0242	8-1-1 Ti	15.2x8.86x0.43	24.4	Free Free	STD. Pebble 6.35	376	Deformation and Pitted Surface	0.10
3-0243	8-1-1 Ti	15.2x8.86x0.43	24.4	Free Free	STD. Pebble 6.35	427	Deformation and Pitted Surface	0.53
3-0244	8-1-1 Ti	15.2x8.86x0.43	24.4	Free Free	STD. Pebble 6.35	380	Slight Deformation and Pitted Surface	0.08
3-0245	8-1-1 Ti	15.2x8.86x0.43	24.4	Free Free	STD. Pebble 6.35	400	Deformation and Pitted Surface	0.30
3-0246	8-1-1 Ti	15.2x8.86x0.43	41.0	Free Free	STD. Pebble 6.35	293	Deformation and Pitted Surface	0.36
3-0247	8-1-1 Ti	15.2x8.86x0.43	41.0	Free Free	STD. Pebble 6.35	301	Deformation and Pitted Surface	0.71
3-0248	8-1-1 Ti	15.2x8.86x0.43	41.0	Free Free	STD. Pebble 6.35	297	slight Deformation and Pitted Surface	0.66
3-0249	8-1-1 Ti	15.2x8.86x0.43	41.0	Free Free	STD. Pebble 6.35	302	Deformation and Pitted Surface	0.18
3-0250	8-1-1 Ti	15.2x8.86x0.43	41.0	Free Free	STD. Pebble 6.35	299	Deformation and Pitted Surface	0.36
3-0251	8-1-1 Ti	15.2x8.86x0.43	41.0	Free Free	Ice Ball 25.40	382	slight Deformation	0.33
3-0252	8-1-1 Ti	15.2x8.86x0.43	41.0	Free Free	Ice Ball 25.40	280	slight Deformation	2.03
3-0253	8-1-1 Ti	15.2x8.86x0.43	24.4	Free Free	Ice Ball 25.40	350	slight Deformation	0.41
3-0254	8-1-1 Ti	15.2x8.86x0.43	24.4	Free Free	Ice Ball 25.40	357	slight Deformation	0.18
3-0255	8-1-1 Ti	15.2x8.86x0.43	24.4	Free Free	Ice Ball 25.40	388	slight Deformation	0.10

Shot #	Test Specimen	Thickness at Impact Point (mm)	Impact Angle (°)	Support Method	Projectile Type Size (mm)	Velocity (m/s)	Remarks
3-0094	APSI Blade	1.59	90	Cantilever	STD. Pebble 6.35	est. 187	Projectile Broke up on Impact. Partial Penetration-Bulge and Crack.
3-0095	APSI Blade	1.59	90	Cantilever	STD. Pebble 6.35	187	Projectile Broke up on Impact. Partial Penetration-Bulge and Crack.
3-009	APSI Blade	1.59	90	Cantilever	STD. Pebble 6.35	242	Projectile Broke up on Impact Complete Penetration-Bulge and Crack you can see through

Shot#	Material	Size (cm)	Leading Edge Thickness (mm)	Impact Angle (°)	Support Method	Impact Site	Projectile Micro Balloon Gelatin	Impact Mass (gm)	Velocity (m/s)	Remarks and Damage Measurements
2-0069	40355	45.72x5.65x0.46	1.22	36.4	Free Free	Mid Span	Pre Sliced	53.6	193	Plastic Deformation 6.55 cm on L.E. 5.23 cm on T.E.
2-0072	40355	45.72x5.66x0.46	1.22	36.4	Free Free	Mid Span	Pre Sliced	61.1	263	Bent in Half U-shaped
2-0073	40355	45.72x5.66x0.46	1.22	36.4	Free Free	Mid Span	Pre Sliced	71.4	238	Bent in Half U-shaped
2-0074	40355	45.72x5.66x0.46	1.22	51.1	Free Free	Mid Span	Pre Sliced	54.5	185	Plastic Deformation 8.31 cm on L.E. 6.73 cm on T.E.
2-0075	40355	45.72x5.66x0.46	1.22	36.4	Cantilever	Mid Span	Pre Sliced	76.4	235	Plastic Deformation 14.17 cm on L.E. 11.43 cm on T.E. Twist 2.49 cm
2-0076	40355	22.86x5.66x0.46	1.22	36.4	Free Free	Mid Span	Pre Sliced	65.7-	236	Bent in Half U-shaped
2-0077	40355	22.86x5.66x0.46	1.22	51.1	Free Free	Mid Span	Pre Sliced	44.2	177	Plastic Deforma. 5.61 cm on L.E. 4.75 cm on T.E. .97 cm bow at tip
2-0078	41055	22.86x5.66x0.21	0.61	51.1	Free Free	Mid Span	Pre Sliced	--	168	Bent and Twisted
2-0079	41055	22.86x5.66x0.21	0.61	36.4	Free Free	Mid Span	Pre Sliced	47.5	245	Bent, Twisted and Mangled
2-0080	40355	22.86x5.66x0.46	1.22	36.4	Free Free	Mid Span	Pre Sliced	45.2	239	Plastic Deformation 0.61 cm on L.E. 0.46 cm on T.E.
2-0081	40355	22.86x5.66x0.46	1.22	25.5	Free Free	Mid Span	Pre Sliced	51.3	182	Plastic Deformation 1.27 cm on L.E. 119 cm on T.E.

Shot#	Material	Size (cm)	Leading Edge Thickness (mm)	Impact Angle (°)	Pre-Stressed Load (lbs)	Impact Site	Projectile Micro Balloon Gelatin	Impact Mass (gm)	Velocity (m/s)	Remarks and Damage Measurements
2-0082	403SS	45.72x5.66x0.46	1.22	51.1	4019	Mid Span	Pre Sliced	56.4	181	Plastic Deformation 2.06 cm on L.E. 0.43 cm on T.E.
2-0083	403SS	45.72x5.66x0.46	1.22	36.4	3245	Mid Span	Pre Sliced	57.3	231	Plastic Deformation 1.83 cm on L.E. 0.36 cm on T.E.
2-0084	410SS	45.72x5.66x0.23	0.61	36.4	1714	Mid Span	Pre Sliced	--	240	Bent and Twisted
2-0085	410SS	45.72x5.66x0.23	0.61	51.1	2025	Mid Span	Pre Sliced	--	--	Plastic Deformation

Shot	T-101 Specimen Material	Size (cm)	Leading Edge Thickness (mm)	Impact Angle (°)	Support Method	Impact Site	Projectile Micro Bal-loon Gelatin	Impact Mass (gm)	Velocity (m/s)	Remarks and Damage Measurements
2-0086	B-1-1 Ti	45.72x8.86x0.41	0.81	36.4	Free Free	Mid Span	Pre Sliced	59.6	248	Plastic Deformation 2.0 cm
2-0087	B-1-1 Ti	45.72x8.86x0.41	0.81	51.1	Free Free	Mid Span	Pre Sliced	54.5	174	No Visual Damage
2-0088	B-1-1 Ti	45.72x8.86x0.41	0.81	24.4	Free Free	Mid Span	Pre Sliced	41.4	370	Plastic Deformation 0.41 cm
2-0089	B-1-1 Ti	45.72x8.86x0.41	0.81	41.0	Free Free	Mid Span	Pre Sliced	16.7	311	No Visual Damage

94

U.S. Government Printing Office: 1982 — 559-002/2036